

## Supporting Information

### Defect Engineering in $\beta$ -ketoenamine Linked Covalent Organic Frameworks for High-Efficiency Uranium Extraction

Douchao Mei and Bing Yan\*

Shanghai Key Lab of Chemical Assessment and Sustainability, School of Chemical Science and Engineering, Tongji University, Siping Road 1239, Shanghai 200092, China

E-mail: byan@tongji.edu.cn

#### Supporting Information

##### Experimental Section

1. Materials
2. Characterization instruments
3. Uranium adsorption study
4. Antibacterial property assay
5. Theoretical calculations

**Figure S1.** Different views of Tp-DAAQ.

**Figure S2.** Different views of Tp-AD.

**Figure S3.** Different views of Tp-DAQ.

**Figure S4.** PXRD patterns of (a) Tp-DAAQ-1, (b) Tp-DAAQ-2, (c) Tp-DAAQ-3 and (d) Tp-DAAQ-4.

**Figure S5.** FT-IR spectrum of Tp-DAAQ.

**Figure S6.** FT-IR spectra of (a) Tp-DAAQ-1, (b) Tp-DAAQ-2, (c) Tp-DAAQ-3 and (c) Tp-DAAQ-4.

**Figure S7.** High-resolution C 1s XPS spectra of (a) Tp-DAAQ, (b) Tp-AD and (c) Tp-DAQ.

**Figure S8.** Thermogravimetric analysis (TGA) curves of (a) Tp-DAAQ, (b) Tp-DAAQ-1, (c) Tp-DAAQ-2, (d) Tp-DAAQ-3 and (e) Tp-DAAQ-4.

**Figure S9.** (a, b) SEM images of Tp-DAAQ and (c, d, e, f) SEM-EDS mapping images of Tp-DAAQ.

**Figure S10.** (a, b, c, d) TEM images of Tp-DAAQ.

**Figure S11.** (a, b) SEM images of Tp-DAAQ-1 and (c, d, e, f) SEM-EDS mapping images of Tp-DAAQ-1.

**Figure S12.** (a, b) SEM images of Tp-DAAQ-2 and (c, d, e, f) SEM-EDS mapping images of Tp-DAAQ-2.

**Figure S13.** (a, b) SEM images of Tp-DAAQ-3 and (c, d, e, f) SEM-EDS mapping images of Tp-DAAQ-3.

**Figure S14.** (a, b) SEM images of Tp-DAAQ-4 and (c, d, e, f) SEM-EDS mapping images of Tp-DAAQ-4.

**Figure S15.** FT-IR spectrum of Tp-AD.

**Figure S16.** PXRD patterns of (a) Tp-AD-1, (b) Tp-AD-2, (c) Tp-AD-3 and (d) Tp-AD-4.

**Figure S17.** FT-IR spectra of (a) Tp-AD-1, (b) Tp-AD-2, (c) Tp-AD-3 and (d) Tp-AD-4.

**Figure S18.** Thermogravimetric analysis (TGA) curves of (a) Tp-AQ, (b) Tp-AD-1, (c) Tp-AD-2, (d) Tp-AD-3 and (e) Tp-AD-4.

**Figure S19.** (a, b) SEM images of Tp-AD and (c, d, e, f) SEM-EDS mapping images of Tp-AD.

**Figure S20.** (a, b, c, d) TEM images of Tp-AD.

**Figure S21.** (a, b) SEM images of Tp-AD-1 and (c, d, e, f) SEM-EDS mapping images of Tp-AD-1.

**Figure S22.** (a, b) SEM images of Tp-AD-2 and (c, d, e, f) SEM-EDS mapping images of Tp-AD-2.

**Figure S23.** (a, b) SEM images of Tp-AD-3 and (c, d, e, f) SEM-EDS mapping images of Tp-AD-3.

**Figure S24.** (a, b) SEM images of Tp-AD-4 and (c, d, e, f) SEM-EDS mapping images of Tp-AD-4.

**Figure S25.** FT-IR spectrum of Tp-DAQ.

**Figure S26.** Thermogravimetric analysis (TGA) curves of Tp-DAQ.

**Figure S27.** (a, b) SEM images of Tp-DAQ and (c, d, e, f) SEM-EDS mapping images of Tp-DAQ.

**Figure S28.** TEM images of Tp-DAQ.

**Figure S29.** PXRD patterns of (a) Tp-DAAQ, (b) Tp-AD and (c) Tp-DAQ after being immersed in different pH solutions for 24 h and (d) PXRD pattern of Tp-DAQ after being immersed in different pH solutions for 72 h.

**Figure S30.** Effect of pH for the uranium adsorption on Tp-DAAQ, Tp-AD and Tp-DAQ ( $C_0 = 100 \text{ ppm}$  and  $m/V = 1/10 \text{ g}\cdot\text{L}^{-1}$ ).

**Figure S31.** Zeta potential of (a) Tp-DAAQ, (b) Tp-AD and (c) Tp-DAQ at the pH range of 3-8.

**Figure S32.** (a) Adsorption selectivity study of Tp-AD for gold ( $C_{\text{single metal ion}} = 100 \text{ mg}\cdot\text{L}^{-1}$  and  $t = 12 \text{ h}$ ) and (b) comparison of distribution coefficient ( $K_d$ ) of Tp-AD for different metal ions ( $C_0 = 100 \text{ mg}\cdot\text{L}^{-1}$ ,  $\text{pH} = 6$ ,  $m/V = 1/10 \text{ g}\cdot\text{L}^{-1}$  and  $t = 12 \text{ h}$ ).

**Figure S33.** Adsorption kinetics curve of Tp-DAAQ fitting with Weber-Morris model.

**Figure S34.** Adsorption kinetics curve of Tp-AD fitting with Weber-Morris model.

**Figure S35.** Adsorption kinetics curve of Tp-DAQ fitting with (a) pseudo-first-order and pseudo-second-order models and (b) Weber-Morris model.

**Figure S36.** Adsorption isotherm curve of Tp-DAAQ fitting with D-R model.

**Figure S37.** Adsorption isotherm curve of Tp-AD fitting with D-R model.

**Figure S38.** Adsorption isotherm curve of Tp-DAQ fitting with (a) Langmuir model as well as Freundlich model and (b) D-R model.

**Figure S39.** (a) The relation between temperature and adsorption capacity of Tp-DAAQ for uranium; (b) linear curve of  $\ln K_c$  vs  $1/T$ .

**Figure S40.** (a) The relation between temperature and adsorption capacity of Tp-AD for uranium; (b) linear curve of  $\ln K_c$  vs  $1/T$ .

**Figure S41.** (a) The relation between temperature and adsorption capacity of Tp-DAQ for uranium; (b) linear curve of  $\ln K_c$  vs  $1/T$ .

**Figure S42.** The regeneration cycle of Tp-AD for uranium capture ( $C_0 = 100 \text{ mg}\cdot\text{L}^{-1}$ ,  $\text{pH} = 6$ ,  $m/V = 1/10 \text{ g}\cdot\text{L}^{-1}$  and  $t = 8 \text{ h}$ ).

**Figure S43.** PXRD patterns of (a) Tp-DAAQ, (b) Tp-AD and (c) Tp-DAQ before and after uranium adsorption.

**Figure S44.** FT-IR spectra of (a) Tp-DAAQ and (b) Tp-AD before and after regeneration.

**Figure S45.** PXRD patterns of (a) Tp-DAAQ and (b) Tp-AD before and after regeneration.

**Figure S46.** The extraction efficiency of Tp-DAAQ for uranium in actual water environments.

**Figure S47.** (a) SEM images and (b) SEM-EDS of Tp-DAAQ-U.

**Figure S48.** (a, b, c, d, e) SEM-EDS mapping of Tp-DAAQ-U.

**Figure S49.** (a) SEM images and (b) SEM-EDS of Tp-AD-U.

**Figure S50.** (a, b, c, d, e) SEM-EDS mapping of Tp-AD-U.

**Figure S51.** (a) SEM images and (b) SEM-EDS of Tp-DAQ-U.

**Figure S52.** (a, b, c, d, e) SEM-EDS mapping of Tp-DAQ-U.

**Figure S53.** XPS profiles of (a) Tp-DAAQ, (b) Tp-AD and (c) Tp-DAQ before and after uranium adsorption.

**Figure S54.** High-resolution U 4f XPS spectra of (a) Tp-DAAQ, (b) Tp-AD and (c) Tp-DAQ after uranium adsorption.

**Figure S55.** High-resolution (a) N 1s and (b) O 1s XPS spectra of Tp-DAAQ before and after uranium adsorption.

**Figure S56.** High-resolution (a) N 1s and (b) O 1s XPS spectra of Tp-AD before and after uranium adsorption.

**Figure S57.** High-resolution (a) N 1s and (b) O 1s XPS spectra of Tp-DAQ before and after uranium adsorption.

**Figure S58.** Mulliken atomic charge distributions of (a) Tp-DAAQ, (b) Tp-AD and (c) Tp-DAQ.

**Figure S59.** Agar plate images of MRSA after incubation with different formulations.

**Figure S60.** Agar plate images of *S. aureus* after incubation with different formulations.

**Figure S61.** Effect of coexisting ions for the uranium extraction on Tp-DAAQ and Tp-AD.

**Figure S62.** Effect of different competing anions for the uranium extraction by Tp-DAAQ and Tp-AD.

**Table S1.** Fractional atomic coordinates of Tp-DAAQ.

**Table S2.** Fractional atomic coordinates of Tp-AD.

**Table S3.** Fractional atomic coordinates of Tp-DAQ.

**Table S4.** The atomic percentages of Tp-DAAQ, Tp-AD and Tp-DAQ before and after being immersed with uranium solution determined by XPS.

**Table S5.** N<sub>2</sub> adsorption/desorption data of Tp-DAAQ, Tp-DAAQ-1, Tp-DAAQ-2, Tp-DAAQ-3, Tp-DAAQ-4, Tp-AD, Tp-AD-1, Tp-AD-2, Tp-AD-3, Tp-AD-4 and Tp-DAQ.

**Table S6.** Uranium adsorption kinetic models onto Tp-DAAQ, Tp-AD and Tp-DAQ.

**Table S7.** Uranium adsorption isotherm models onto Tp-DAAQ, Tp-AD and Tp-DAQ.

**Table S8.** The thermodynamic parameters for uranium adsorption on Tp-DAAQ, Tp-AD and Tp-DAQ.

**Table S9.** The uranium performance comparison of this work and other materials.

## Experimental Section

### 1. Materials

1,3,5-triformylphloroglucinol, 2,6-diaminoanthraquinone, 1,5-diaminoanthraquinone, anthracene-2,6-diamine, acetic acid, uranyl nitrate hexahydrate ( $\text{UO}_2(\text{NO}_3)_2 \cdot 6\text{H}_2\text{O}$ ), ethanol ( $\text{CH}_3\text{CH}_2\text{OH}$ ), 1,4-dioxane, 1,3,5-trimethylbenzene, tetrahydrofuran (THF), acetone, N, N-dimethylformamide (DMF), N, N-Dimethylacetamide (DMAc), nitric acid ( $\text{HNO}_3$ ) and sodium carbonate ( $\text{Na}_2\text{CO}_3$ ) were all purchased from Tansoole or Innochem. *Staphylococcus aureus* (*S. aureus*), *Escherichia coli* (*E. coli*), methicillin-resistant staphylococcus aureus (MRSA) and *Pseudoalteromonas marina* (*P. marina*) were purchased from Shanghai Biological Resources Collection Center. Deionized water was used throughout the experiments. All reagents were used as received without further purification.

### 2. Characterization instruments

Powder X-ray diffraction (PXRD) patterns were collected using a Bruker D8 Advance diffractometer with  $\text{Cu K}\alpha$  radiation at 40 kV and 40 mA. Fourier transform infrared spectra (FT-IR) of the powder samples were obtained on a Nicolet IS10 infrared spectrum radiometer using ATR annex. The morphologies and elemental analysis were obtained by using scanning electronic microscopy (SEM, ZEISS Sigma 300) and transmission electron microscopy (TEM, JEM-F200). Thermogravimetric analysis (TGA) was carried out on a TGA 55 system analyzer under an  $\text{N}_2$  atmosphere at a heating rate of  $10^\circ\text{C}\cdot\text{min}^{-1}$  within the temperature ranging from 25 to  $600^\circ\text{C}$ . Solid-state  $^{13}\text{C}$  cross-polarization magic-angle spinning ( $^{13}\text{C}$  CP/MAS NMR) spectra were recorded by a Bruker Avance II400 spectrometer with a 4-mm double-resonance MAS probe; a sample spinning rate of 10.0 kHz, a contact time of 3 ms (ramp 100), and a pulse delay of 3 s were applied. Nitrogen adsorption/desorption isotherms were measured by a Tristar 2460 analyzer at the liquid nitrogen temperature. The samples were outgassed at  $120^\circ\text{C}$  for 5 h before the measurements. The Brunauer Emmett Teller (BET) method was used to calculate the surface area from the adsorption data. The pore-size-distribution curves were obtained via the non-local density functional theory (NLDFT) method. X-ray photoelectron spectroscopy (XPS) was conducted at a Thermo Scientific K-Alpha photoelectron spectrometer. The fitting curve was carried out with the XPSPEAK41 program. Laser confocal microscopy (LSM 900) was used with for the bacterial staining experiments. Electron spin resonance (ESR) measurements were obtained using a spectrometer (Bruker A300, Germany) to confirm the generation of  $\cdot\text{OH}$  and  $\cdot\text{O}_2^-$  under visible light at room temperature. The concentration of  $\text{UO}_2^{2+}$  and other metal ions were determined using an inductively coupled plasma optical emission spectrometer (ICP-OES, PerkinElmer, Optima 8300). Before ICP-OES test,  $\text{UO}_2^{2+}$  standard curves were determined using standard solutions with concentrations of 0, 1, 5 and 10 ppm, respectively.

### 3. Uranium adsorption experiments

The uranium adsorption experiments were carried out using the batch technique. The uranium aqueous solutions with different concentrations were obtained by diluting the stock solution of  $\text{UO}_2(\text{NO}_3)_2 \cdot 6\text{H}_2\text{O}$  with deionized water. The pH values were adjusted with 0.1 M  $\text{HNO}_3$  and 0.1 M  $\text{Na}_2\text{CO}_3$ . Tp-DAAQ-1, Tp-DAAQ-2, Tp-DAAQ, Tp-DAAQ-3, Tp-DAAQ-4, Tp-AD-1, Tp-AD-2, Tp-AD, Tp-AD-3, Tp-AD-4, or Tp-DAQ sample was added into the working solution with a certain concentration. The concentration of uranium was determined by ICP-OES, after filtered through  $0.45\ \mu\text{m}$  filter membrane. The adsorption capacity and removal rate are calculated on the basis of Eq. (S1) and (S2):

$$Q_e = \frac{(C_0 - C_e)v}{m} \quad \text{S1}$$

$$R = \frac{C_0 - C_e}{C_0} \times 100\% \quad \text{S2}$$

Where  $Q_e$  ( $\text{mg}\cdot\text{g}^{-1}$ ) is equilibrium adsorption capacity,  $R$  is removal rate,  $C_0$  ( $\text{mg}\cdot\text{L}^{-1}$ ) is the initial concentration and  $C_e$  ( $\text{mg}\cdot\text{L}^{-1}$ ) is the equilibrium concentration of  $\text{UO}_2^{2+}$ ,  $m$  is the mass of adsorbent ( $\text{g}$ ),  $V$  ( $\text{L}$ ) is the volume of solution.

### 3.1 Effect of pH for U(VI) adsorption

100 ppm  $\text{UO}_2^{2+}$  solution was adjusted by  $\text{HNO}_3$  and  $\text{Na}_2\text{CO}_3$  to pH values of 3, 4, 5, 6 and 7. At each pH, three parallel experiments were carried out. 30 mL of the solution and 3 mg of COFs were added to each conical flask. The conical flasks were then shaken at 140 rpm for 8 h. The adsorbent was then filtered by 0.45  $\mu\text{m}$  syringe filter units.

### 3.2 Adsorption kinetics

3 mg of COF material was suspended in U(VI) solution (30 mL, 100 ppm) from 1 to 480 min. Samples were withdrawn at fixed time intervals and filtered, and the concentration of  $\text{UO}_2^{2+}$  in the filtrate was examined by ICP-OES analysis. Pseudo-first-order model, pseudo-second-order model and Weber-Morris (W-M) model were used to investigate adsorption kinetics of Tp-DAAQ, Tp-AD and Tp-DAQ toward  $\text{UO}_2^{2+}$ .

Pseudo-first-order kinetic model, pseudo-second-order kinetic model and W-M model were described by the Equation (S3), (S4) and (S5):

$$\ln(Q_e - Q_t) = \ln Q_e - k_1 t \quad \text{S3}$$

$$\frac{t}{Q_t} = \frac{1}{K_2 Q_e^2} + \frac{t}{Q_e} \quad \text{S4}$$

$$Q_e = k_{ip} \sqrt{t} + C \quad \text{S5}$$

Where  $C_e$  ( $\text{mg}\cdot\text{L}^{-1}$ ) is equilibrium concentration of  $\text{Au}^{3+}$ ,  $Q_t$  and  $Q_e$  ( $\text{mg}\cdot\text{g}^{-1}$ ) are the adsorption amount of  $\text{UO}_2^{2+}$  at  $t$  time and after reaching equilibrium, respectively.  $k_1$  ( $\text{min}^{-1}$ ) and  $k_2$  ( $\text{mg}\cdot\text{g}^{-1}$ ) are the rate constants of the pseudo first and second order kinetic models, and  $K_{ip}$  stands for internal diffusion constant.

### 3.3 Adsorption isotherm

3 mg COF was added to 30 mL U(VI) solutions with initial concentrations of 10, 50, 100, 200, 300 and 400 ppm, and then stirred for 8 h at 25 °C. The treated solution was filtered through a 0.45  $\mu\text{m}$  membrane filter, and the filtrate was collected and analyzed by using ICP-OES to determine the remaining U(VI) content.

The Langmuir isotherm is based on the assumption that the adsorbate can only be adsorbed in a single layer on the adsorbent. The fitting of the Langmuir isotherm model is represented by Equation (S6):

$$Q_e = \frac{Q_m C_e K_L}{1 + C_e K_L} \quad \text{S6}$$

Where  $Q_m$  ( $\text{mg}\cdot\text{g}^{-1}$ ) is the largest adsorption capacity of U(VI) adsorbed by adsorbent.  $K_L$  ( $\text{L}\cdot\text{mg}^{-1}$ ) is Langmuir equilibrium constant related to the properties and temperature of adsorbents.

The Freundlich model is an empirical equation based on multilayer adsorption on a heterogeneous surface. The fitting of the Freundlich isotherm model is expressed by Equation (S7).

$$Q_e = K_F C_e^{\frac{1}{n}} \quad \text{S7}$$

Both  $K_F$  and  $n$  are adsorption equilibrium constant related to system and temperature.

The Dubinin–Radushkevitch (D-R) model is used to assess adsorption characteristics, which explicitly consider the interaction between adsorbate and adsorbent. The fitting of D-R isotherm model is expressed by Equation (S8) and (S9).

$$\ln Q_e = \ln Q_m - \beta \varepsilon^2 \quad \text{S8}$$

$$\varepsilon = RT \ln (1 + 1/C_e)$$

S9

$\beta$  is the activity coefficient;  $\varepsilon$  is the polanyi potential; R (8.314 J·mol<sup>-1</sup>·K<sup>-1</sup>) is the gas constant.

### 3.4 Adsorption thermodynamics

To further investigate the adsorption mechanism, the thermodynamic parameters, such as standard enthalpy changes ( $\Delta H$ ), standard Gibbs free energy ( $\Delta G$ ) and standard entropy change ( $\Delta S$ ) are calculated by relative adsorption data. The values of  $\Delta H$ ,  $\Delta G$  and  $\Delta S$  can be calculated from the Equation (S10), (S11) and (S12), respectively.

$$k_d = \frac{Q_e}{C_e} = \frac{(C_0 - C_e)}{C_e} \times \frac{v}{m} \quad \text{S10}$$

$$\ln k_d = -\frac{\Delta H}{RT} + \frac{\Delta S}{R} \quad \text{S11}$$

$$\Delta G = \Delta H - T\Delta S \quad \text{S12}$$

Where  $K_d$  is the distribution coefficient.

### 3.5 Adsorption selectivity study

15 conical flasks containing 30 mL Ag, K, Na, Cr, Mg, Ba, Ni, Pb, Cu, Ca, Cd, V, Zn, Co and U solutions (100 ppm) were prepared and COF (3 mg) was added to each conical flask, respectively. In addition, 3 mg COF was added into a mixed solution (30 mL) including K<sup>+</sup>, Na<sup>+</sup>, Mg<sup>2+</sup>, Ba<sup>2+</sup>, Ni<sup>2+</sup>, Pb<sup>2+</sup>, Cu<sup>2+</sup>, Ca<sup>2+</sup>, Cd<sup>2+</sup>, Zn<sup>2+</sup>, Co<sup>2+</sup> and UO<sub>2</sub><sup>2+</sup> to further investigate the selectivity. Furthermore, the effect of competing ions (CO<sub>3</sub><sup>2-</sup>, Cl<sup>-</sup>, NO<sub>3</sub><sup>-</sup> and SO<sub>4</sub><sup>2-</sup>) for the uranium adsorption was also investigated. After shaking at 140 rpm for 12 h, the liquid supernatant was filtered through a 0.45  $\mu$ m membrane filter and the filtrate was analyzed via ICP-OES to determine the residual metal ion concentrations. Comparison of the selectivity toward various metal ions were performed using the Equation (S10):

### 3.6 Recyclability study

At room temperature, Tp-DAAQ (30 mg) and T-AD (30 mg) were added into 300 mL of 100 ppm U(VI) solution and shaken for 8 h. After the adsorption equilibrium was arrived, the remaining suspensions were filtered and the adsorbents were soaked in HNO<sub>3</sub> (0.01M) for 12 h. The desorbed material was washed by deionized water until the eluant became neutral. The obtained solid material by centrifugation was used for the next U(VI) adsorption experiment. The adsorption-desorption processes were repeated for 6 times, and ICP-OES was employed to measure the concentration of filtrate. The adsorption capacity was calculated by using Equation (S1).

### 3.7 U(VI) removal from actual water samples

The real aqueous environments (tap water, river water, simulated seawater, Bohai seawater) were directly used in uranium adsorption experiments without further treatment. The tap water and river water were obtained from Tongji University. 10 mg of Tp-DAAQ or Tp-AD was dispersed into 20 mL of uranium-spiked actual aqueous environments (10 ppm). The pH values of solutions were adjusted to 6 by HNO<sub>3</sub> and Na<sub>2</sub>CO<sub>3</sub>. After 24 h, the removal rate for uranium was recorded, respectively.

## 4. Antibacterial property assay

### 4.1 In vitro antibacterial assay

To evaluate the antibacterial activities of Tp-DAAQ, Tp-AD and Tp-DAQ, gram-negative *E. coli*, gram-positive *S. aureus*, MRSA and *P. marina* were selected as model microorganisms. Before the test of antibacterial activity, *E. coli*, *S. aureus*, MRSA and *P. marina* were diluted to a certain concentration. The diluted bacterial suspensions were mixed with Tp-DAAQ, Tp-AD or Tp-DAQ in a 96-well plate, which was treated with light irradiation for 10 min. In addition, bacteria without any treatment were used as a control. Then, 10  $\mu$ L of the bacterial suspension was

dropped onto the agar plates and spread uniformly. After incubation at 37 °C for 18 h, the viable colonies of bacteria were counted and recorded. The antibacterial activity was calculated using the formula (S13):

$$\text{Antibacterial activity} = \frac{N_0 - N_e}{N_0} \times 100\%$$

S13

Where  $N_0$  is the number of bacterial colonies in the control group and  $N_e$  is the number of bacterial colonies treated with Tp-DAAQ, Tp-AD or Tp-DAQ under visible light irradiation. Each experiment was repeated three times.

#### 4.2 Dead/Live staining assay

Dead/live staining assay was performed to determine the viability of bacteria. First, the bacteria were co-cultured with Tp-DAAQ, Tp-AD or Tp-DAQ for 2 h at 37°C and then irradiated using visible light for 10 min. The supernatant was removed and the sediment was washed three times using PBS. Bacteria were stained using SYTO. 9 and PI for 15 min in the dark and images were captured using a Laser confocal microscopy after washing the stained samples three times with PBS.

#### 4.3 Bacterial characterization using SEM

The bacterial suspensions of *E. coli*, *S. aureus*, MRSA and *P. marina* with/without COF samples were exposed to light irradiation for 10 min. Then, the mixture was incubated for 2 h at 37 °C, Next, the bacterial samples were dehydrated using an 75% ethanol for 10 min. Finally, the obtained samples were used for SEM characterization.

### 5. Theoretical calculations

The adsorption mechanisms of Tp-DAAQ, Tp-AD and Tp-DAQ toward U(VI) were investigated by density functional theory (DFT) calculations according to Gaussian 16 Revision and Materials Studio 2019. The visualization of the orbitals was achieved using Visual Molecular Dynam (VMD) and Multiwfn software (version 3.8).

#### 5.1 Frontier molecular orbitals (FMO) and electrostatic potential (ESP) calculations

The HOMO and LUMO energy levels as well as the molecular ESP were obtained by using Gaussian 16. Geometry optimizations and frequency calculations of Tp-DAAQ, Tp-AD and Tp-DAQ were performed at the B3LYP/6-31G(d) level and the optimized structure was then used to calculate single-point energy at a more precise level of B3LYP/6-31G(d, p). The HOMO-LUMO orbitals and ESP surface map were constructed by the Multiwfn program and VMD.

#### 5.2 Adsorption energy

The adsorption energy was calculated using the DMol3 package in Materials Studio software. Electron-ion interactions were described using the all electron relativistic (AER) potentials. GGA-PBE function and DNP4.4 basis set was employed in the process of calculation. During the geometry optimizations, the convergence criterion for the electronic self-consistent field (SCF) loop was set to  $10^{-6}$ . The atomic structures were optimized until the energy change was below  $10^{-5}$  Ha, and the maximum force was below 0.002 Ha/Å and maximum displacements was below 0.005 Å

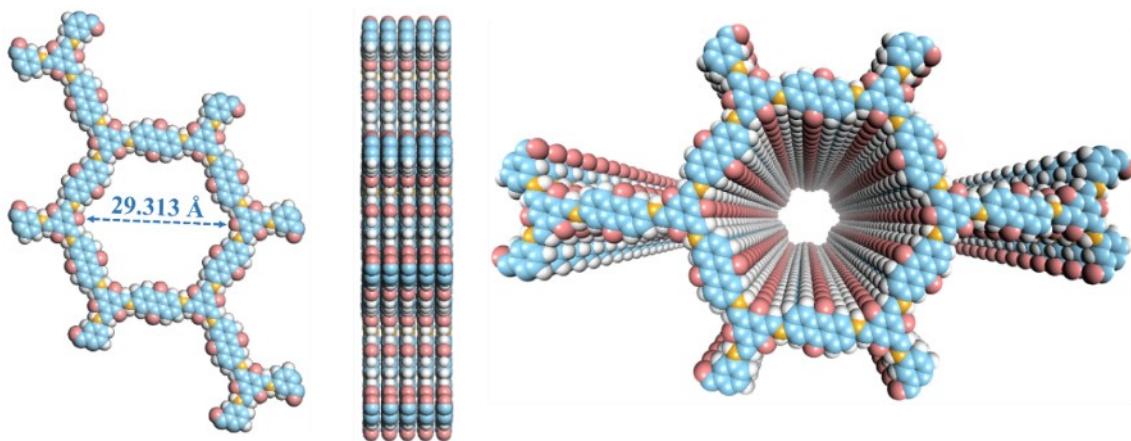


**Figure S1.** Different views of Tp-DAAQ.

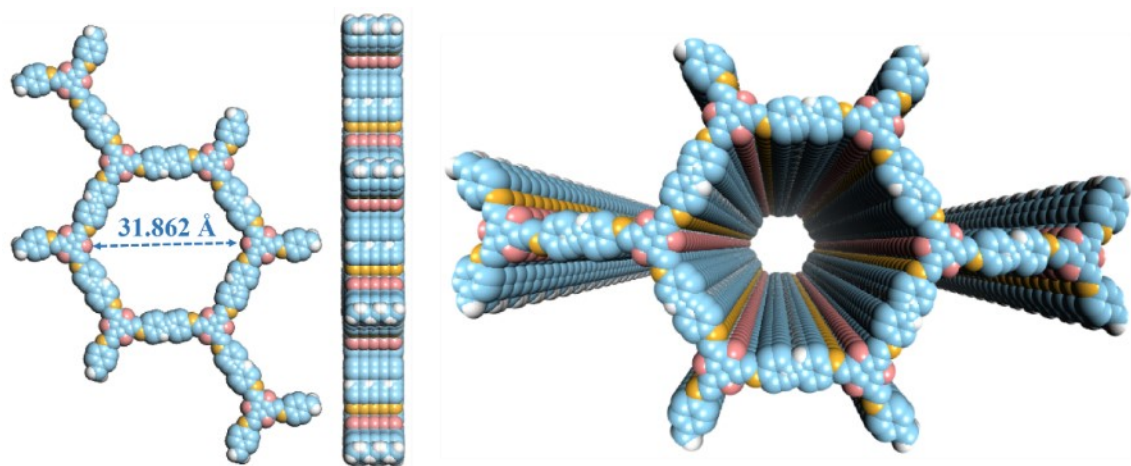


**Figure S2.** Different views of Tp-AD.

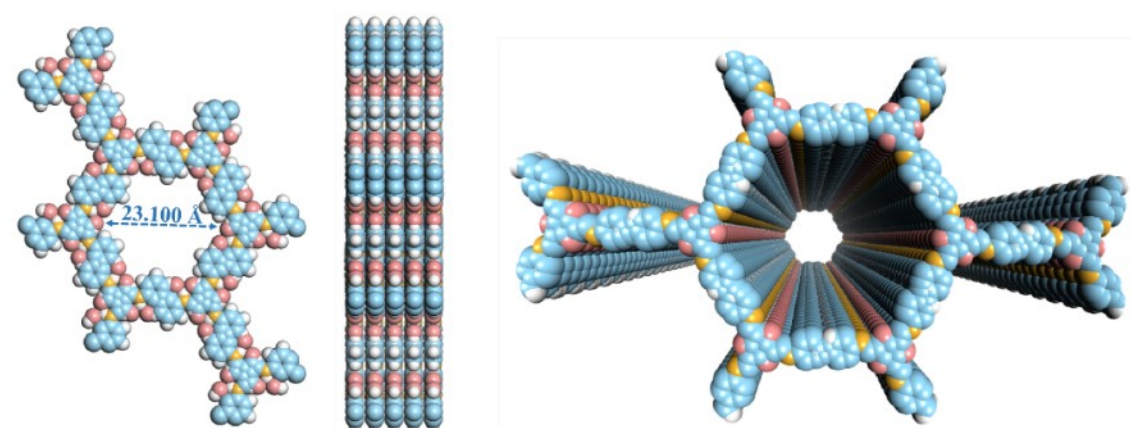


**Figure S3.** Different views of Tp-DAQ.

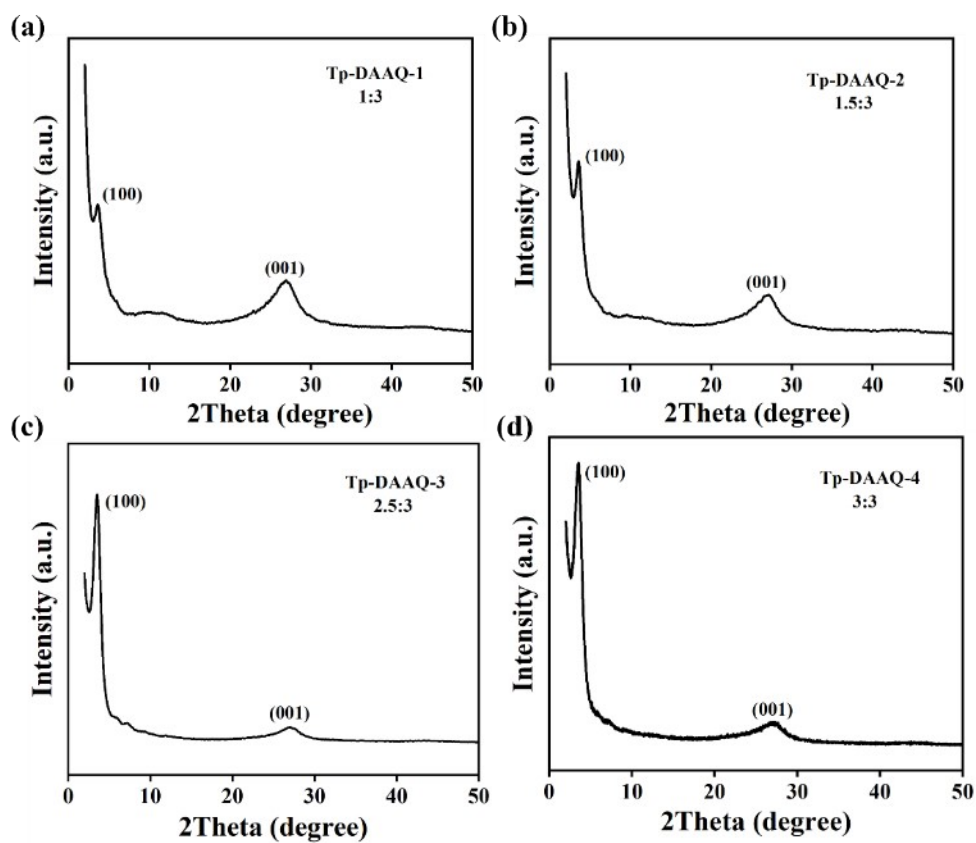


**Figure S4.** PXRD patterns of (a) Tp-DAAQ-1, (b) Tp-DAAQ-2, (c) Tp-DAAQ-3 and (d) Tp-DAAQ-4.

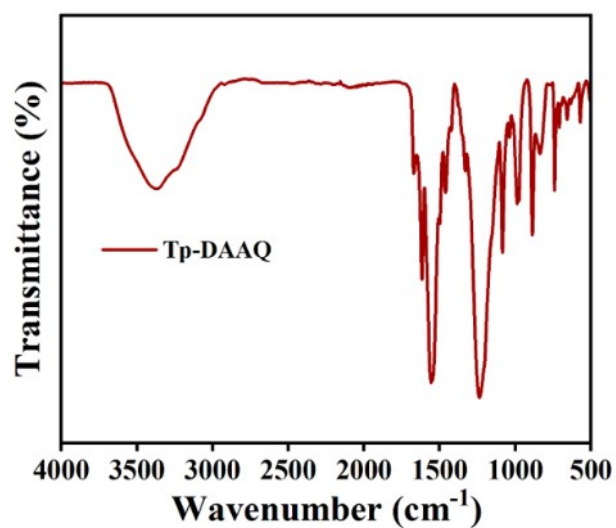


**Figure S5.** FT-IR spectrum of Tp-DAAQ.

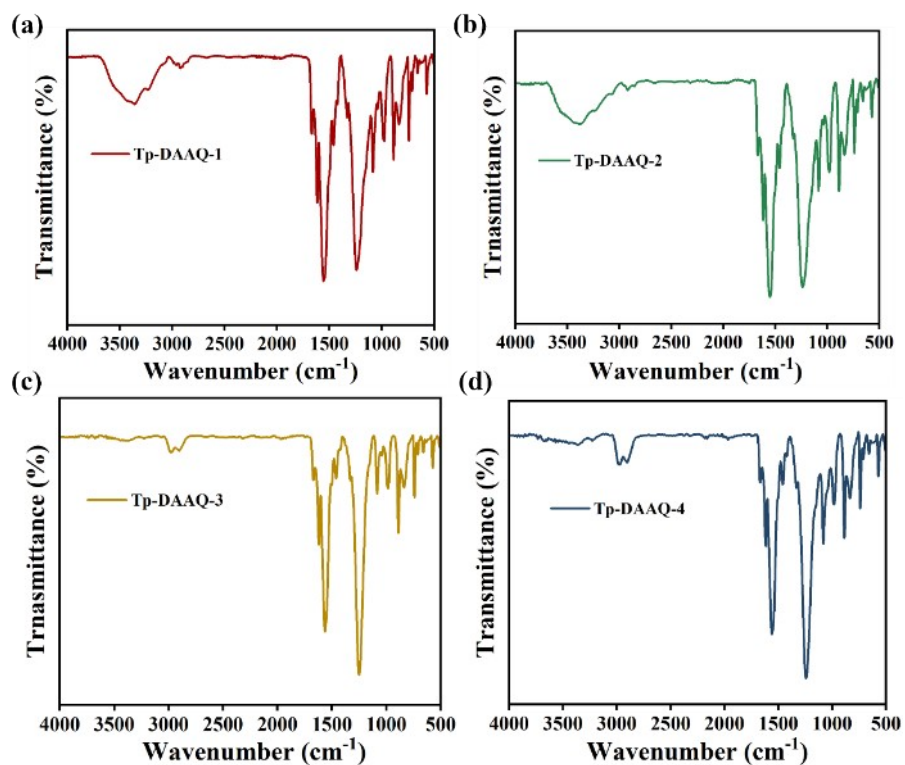


**Figure S6.** FT-IR spectra of (a) Tp-DAAQ-1, (b) Tp-DAAQ-2, (c) Tp-DAAQ-3 and (c) Tp-DAAQ-4.

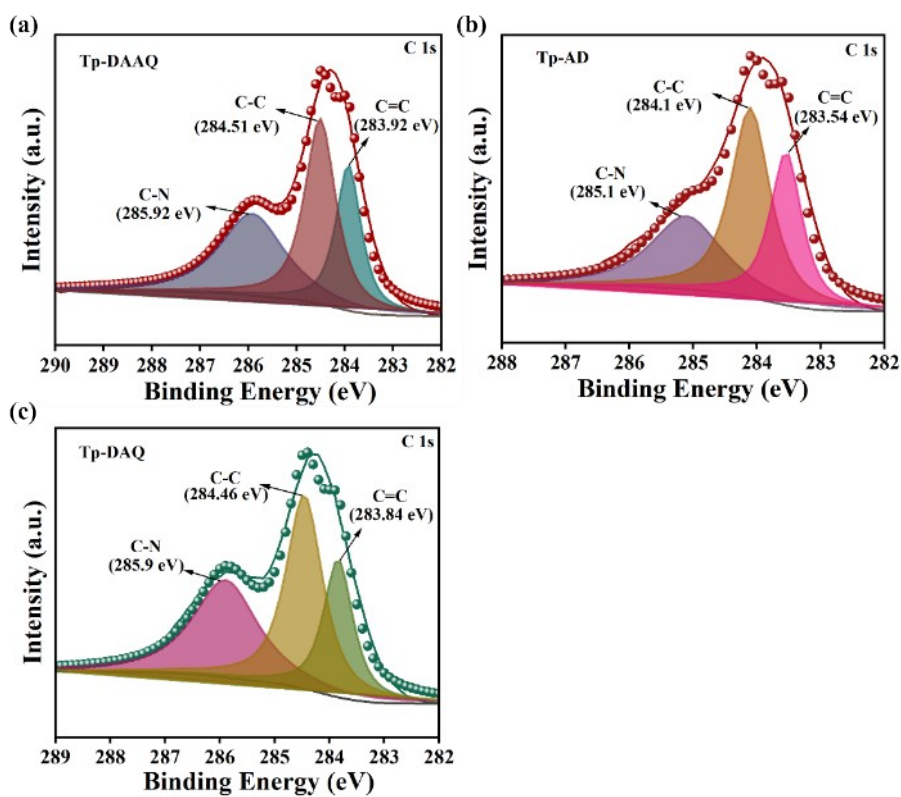


**Figure S7.** High-resolution C 1s XPS spectra of (a) Tp-DAAQ, (b) Tp-AD and (c) Tp-DAQ.

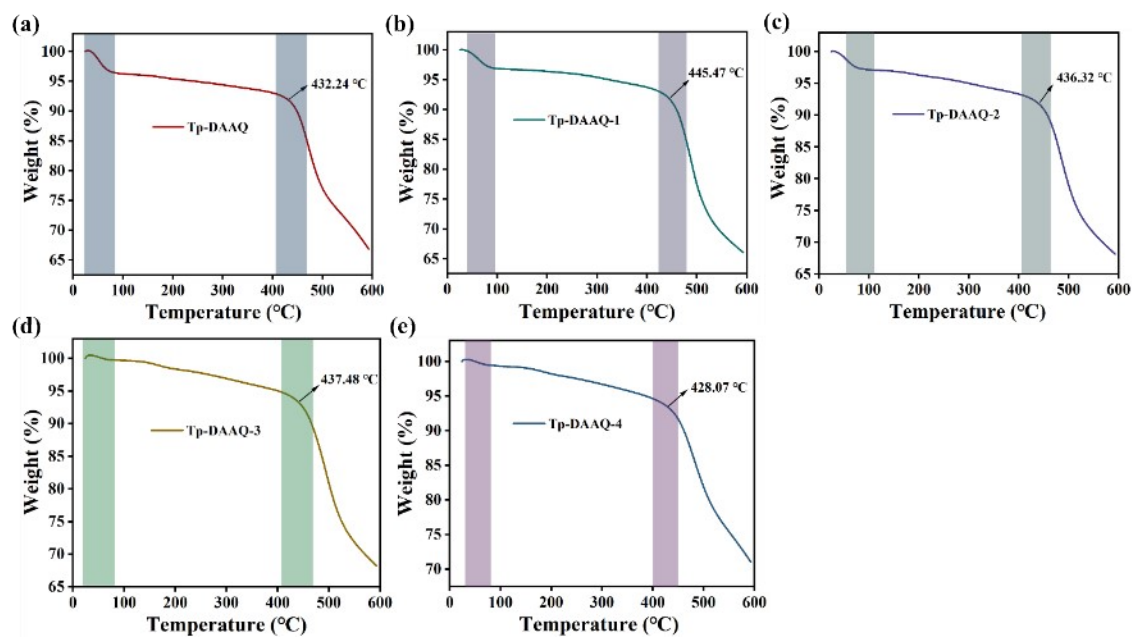


**Figure S8.** Thermogravimetric analysis (TGA) curves of (a) Tp-DAAQ, (b) Tp-DAAQ-1, (c) Tp-DAAQ-2, (d) Tp-DAAQ-3 and (e) Tp-DAAQ-4.

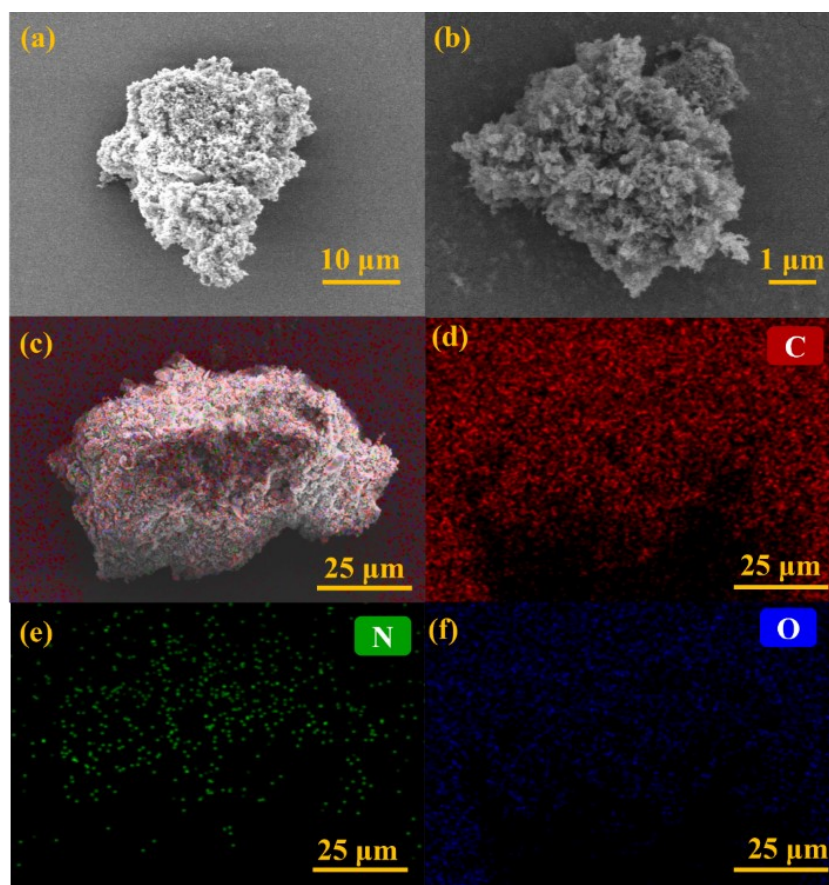


**Figure S9.** (a, b) SEM images of Tp-DAAQ and (c, d, e, f) SEM-EDS mapping images of Tp-DAAQ.

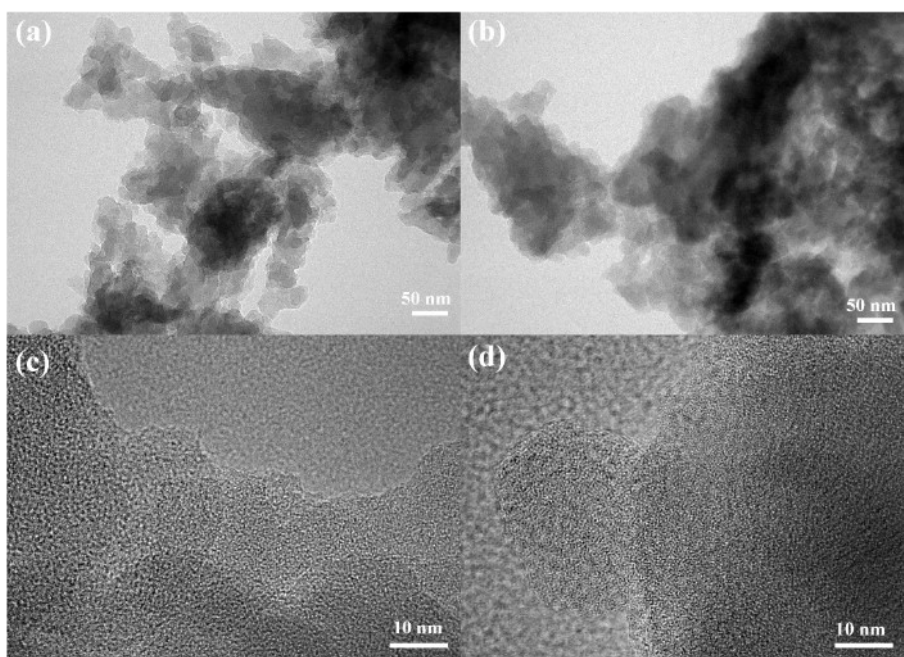


**Figure S10.** (a, b, c, d) TEM images of Tp-DAAQ.

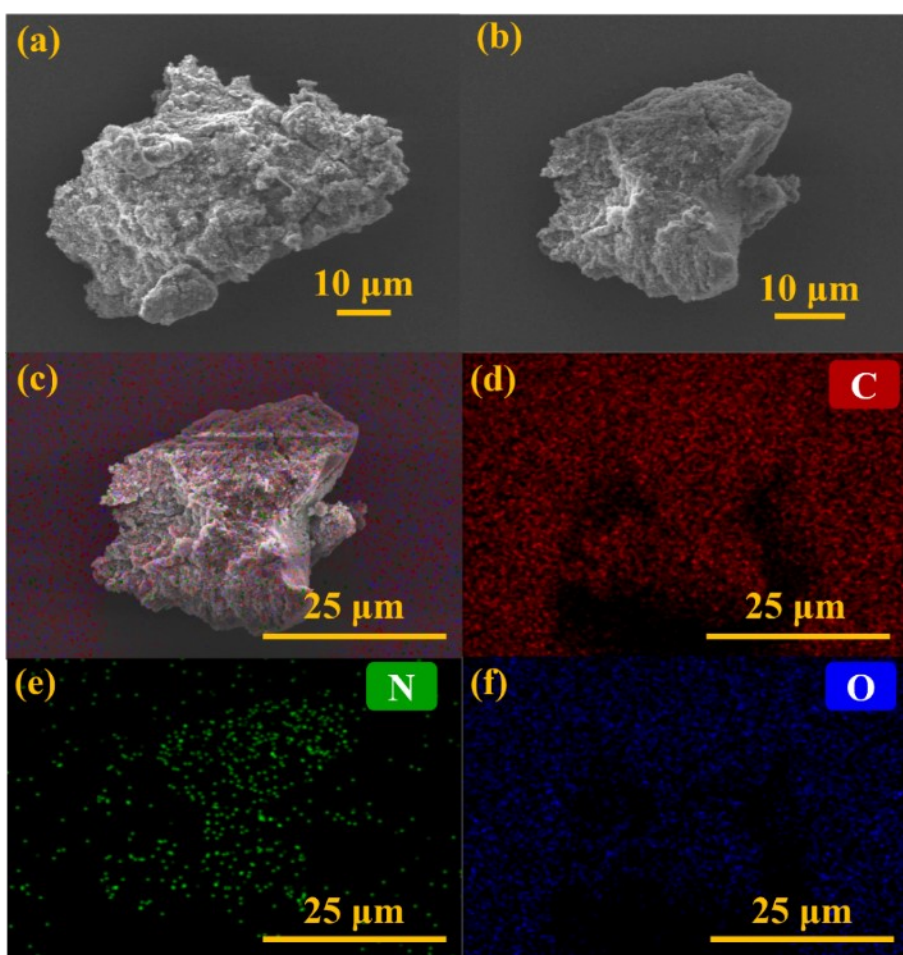


**Figure S11.** (a, b) SEM images of Tp-DAAQ-1 and (c, d, e, f) SEM-EDS mapping images of Tp-DAAQ-1.

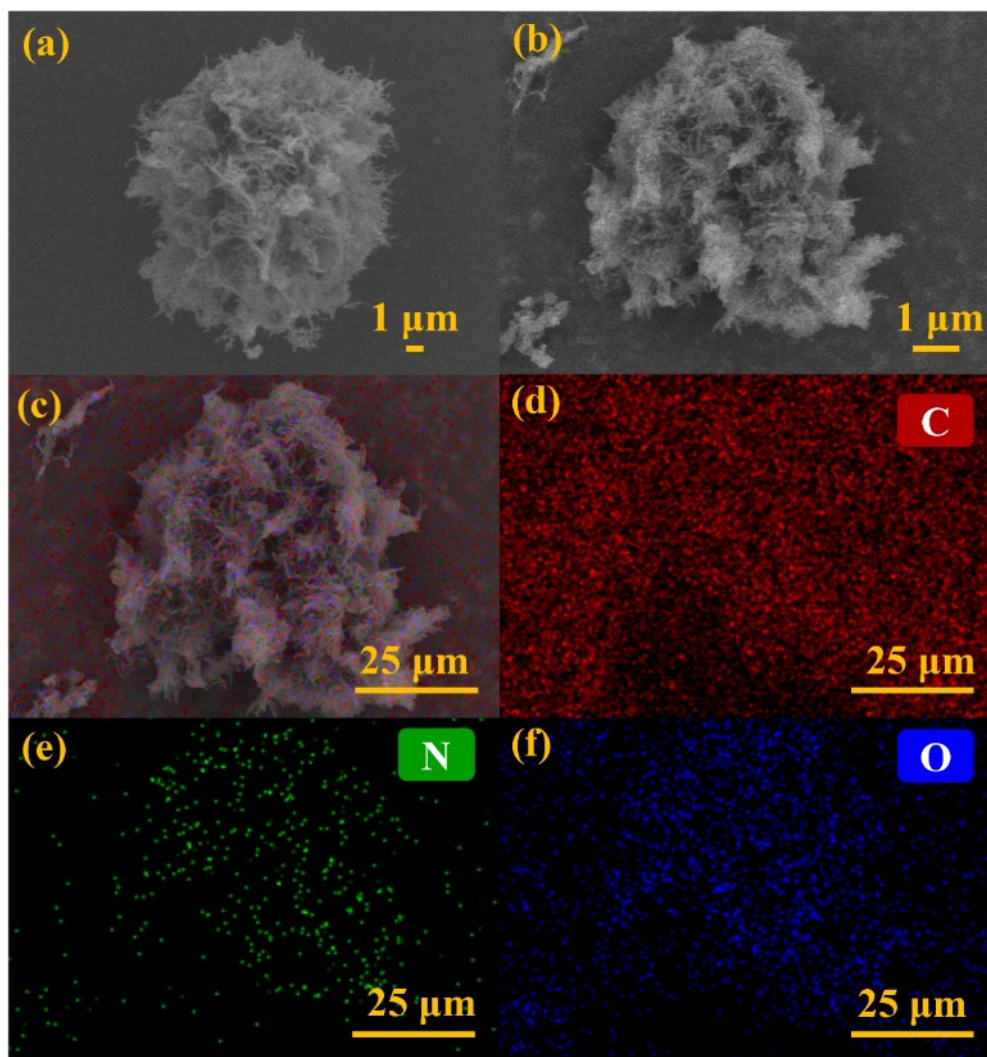


**Figure S12.** (a, b) SEM images of Tp-DAAQ-2 and (c, d, e, f) SEM-EDS mapping images of Tp-DAAQ-2.

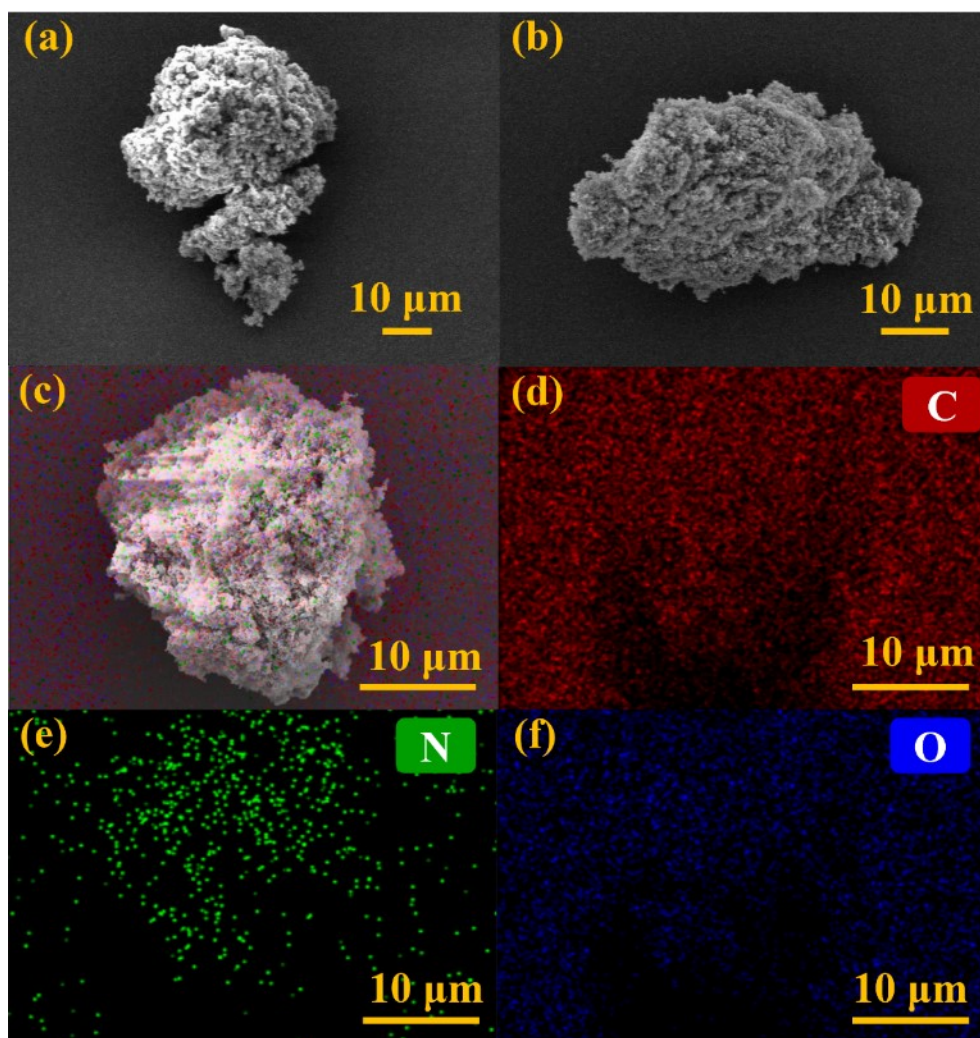


**Figure S13.** (a, b) SEM images of Tp-DAAQ-3 and (c, d, e, f) SEM-EDS mapping images of Tp-DAAQ-3.

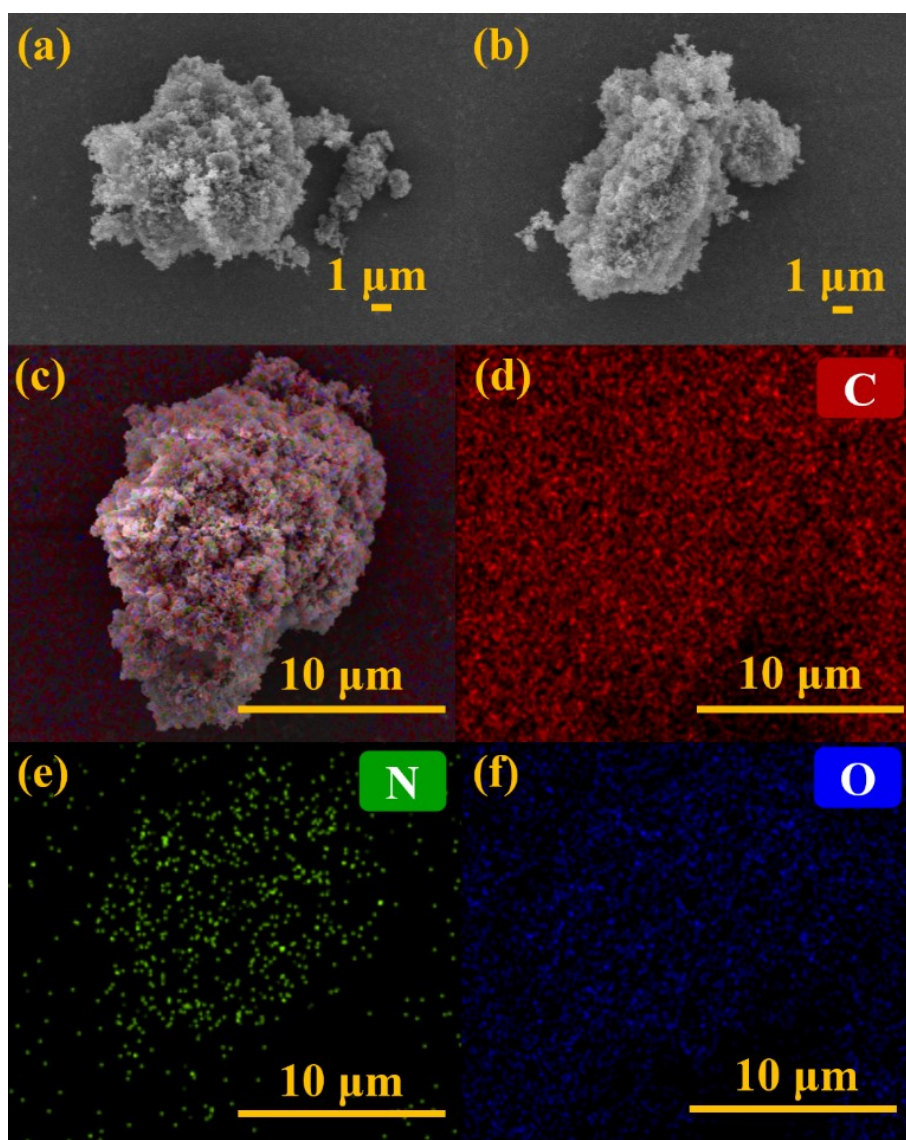


**Figure S14.** (a, b) SEM images of Tp-DAAQ-4 and (c, d, e, f) SEM-EDS mapping images of Tp-DAAQ-4.

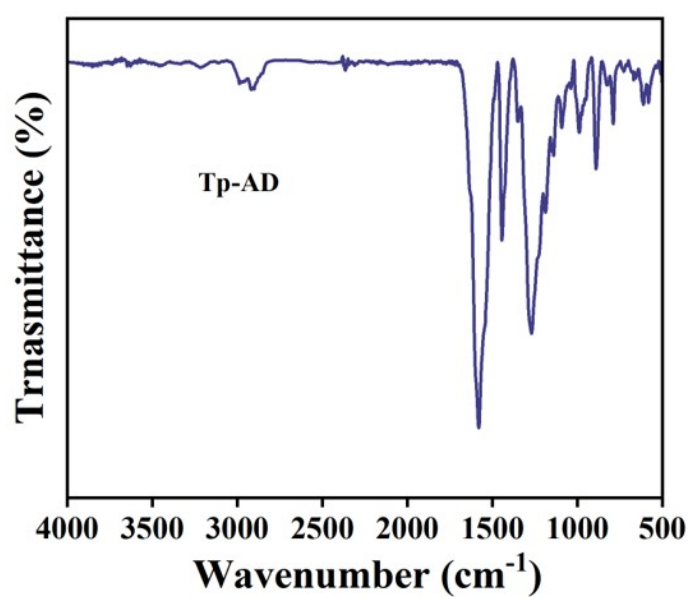


**Figure S15.** FT-IR spectrum of Tp-AD.

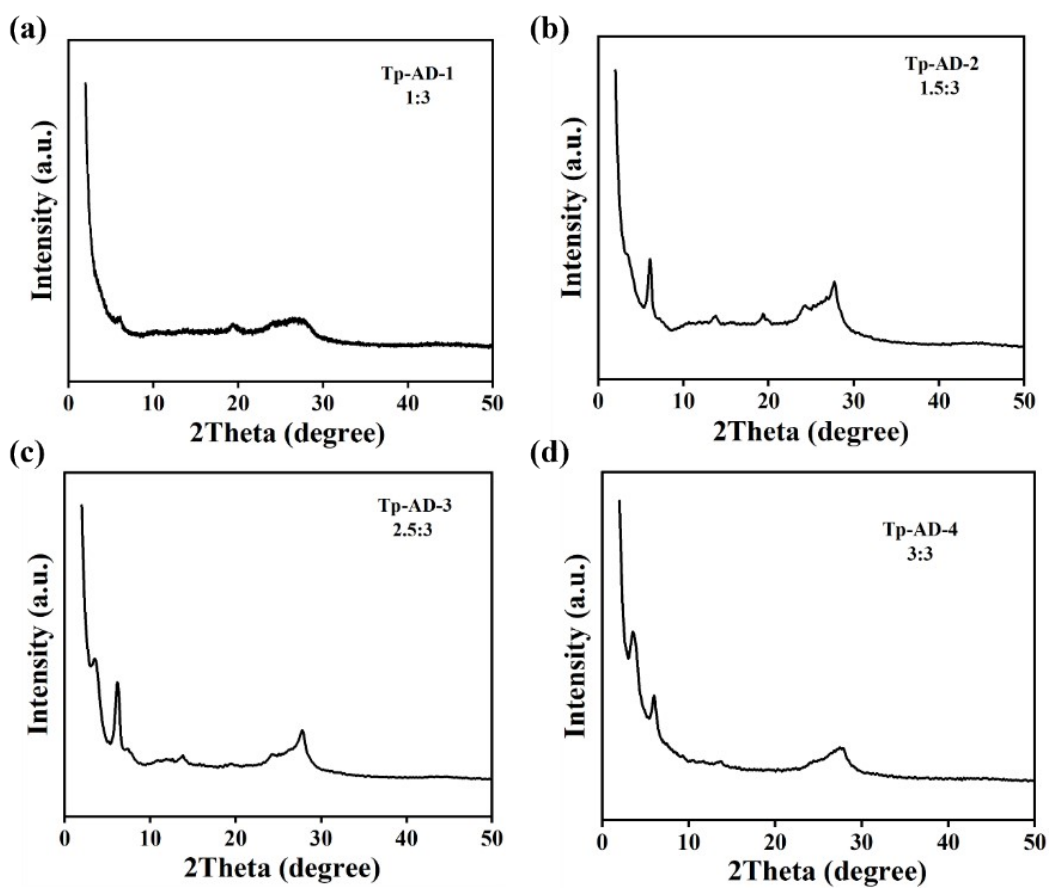


Figure S16. PXRD patterns of (a) Tp-AD-1, (b) Tp-AD-2, (c) Tp-AD-3 and (d) Tp-AD-4.

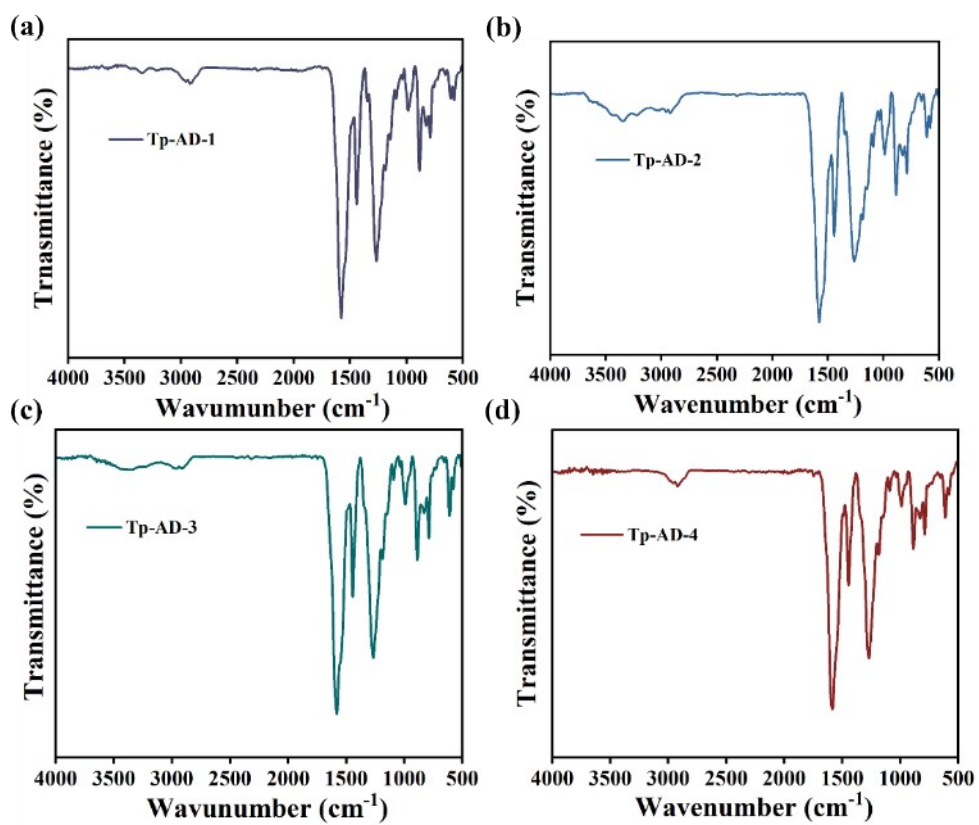
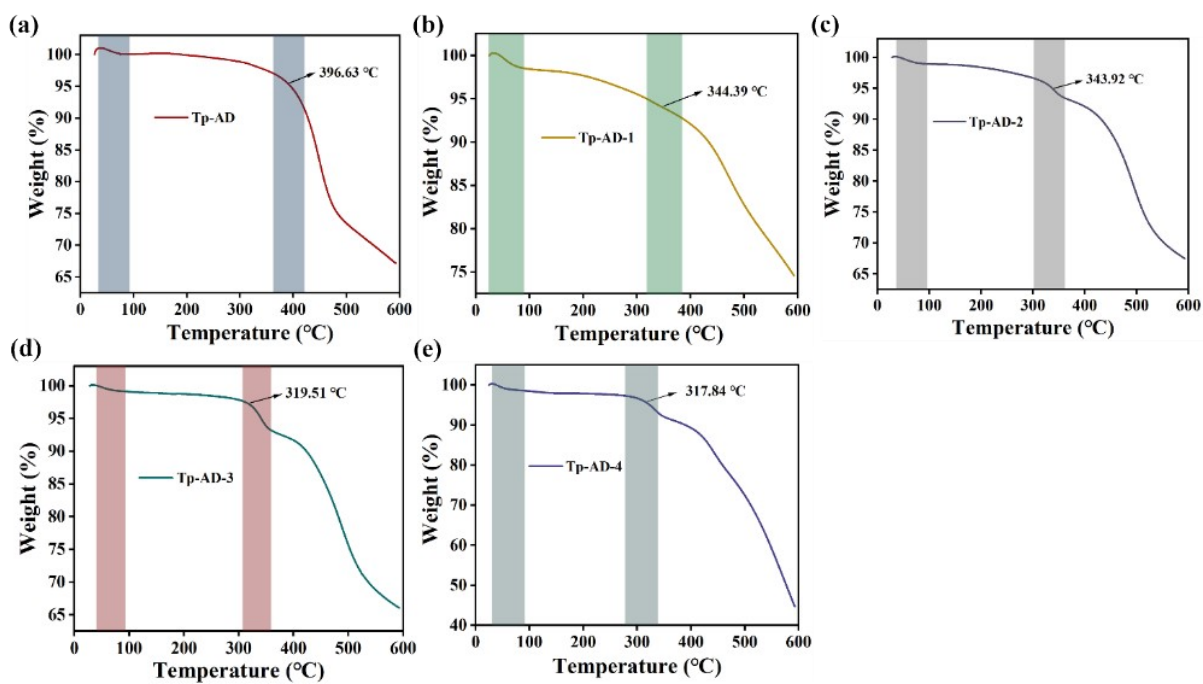
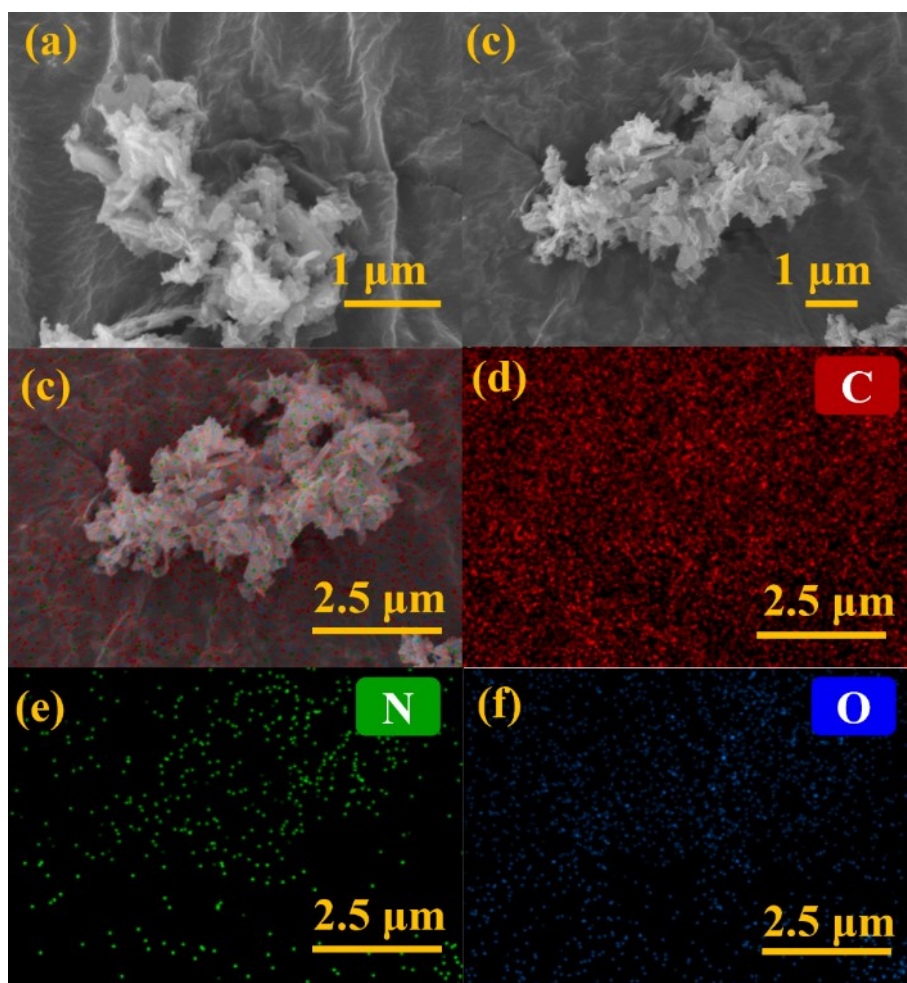


Figure S17. FT-IR spectra of (a) Tp-AD-1, (b) Tp-AD-2, (c) Tp-AD-3 and (d) Tp-AD-4.



**Figure S18.** Thermogravimetric analysis (TGA) curves of (a) Tp-AQ, (b) Tp-AD-1, (c) Tp-AD-2, (d) Tp-AD-3 and (e) Tp-AD-4.



**Figure S19.** (a, b) SEM images of Tp-AD and (c, d, e, f) SEM-EDS mapping images of Tp-AD.

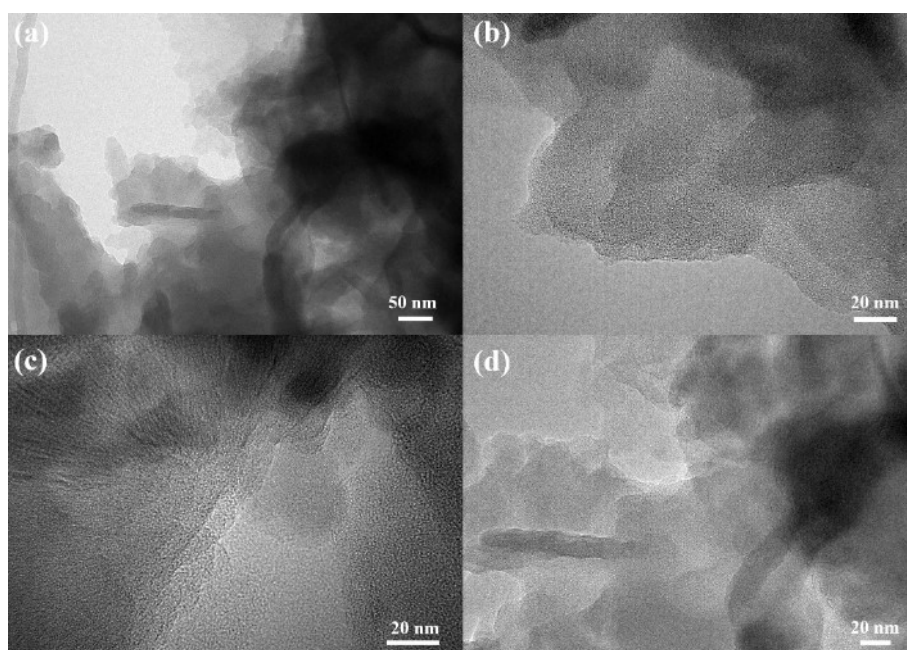


**Figure S20.** (a, b, c, d) TEM images of Tp-AD.

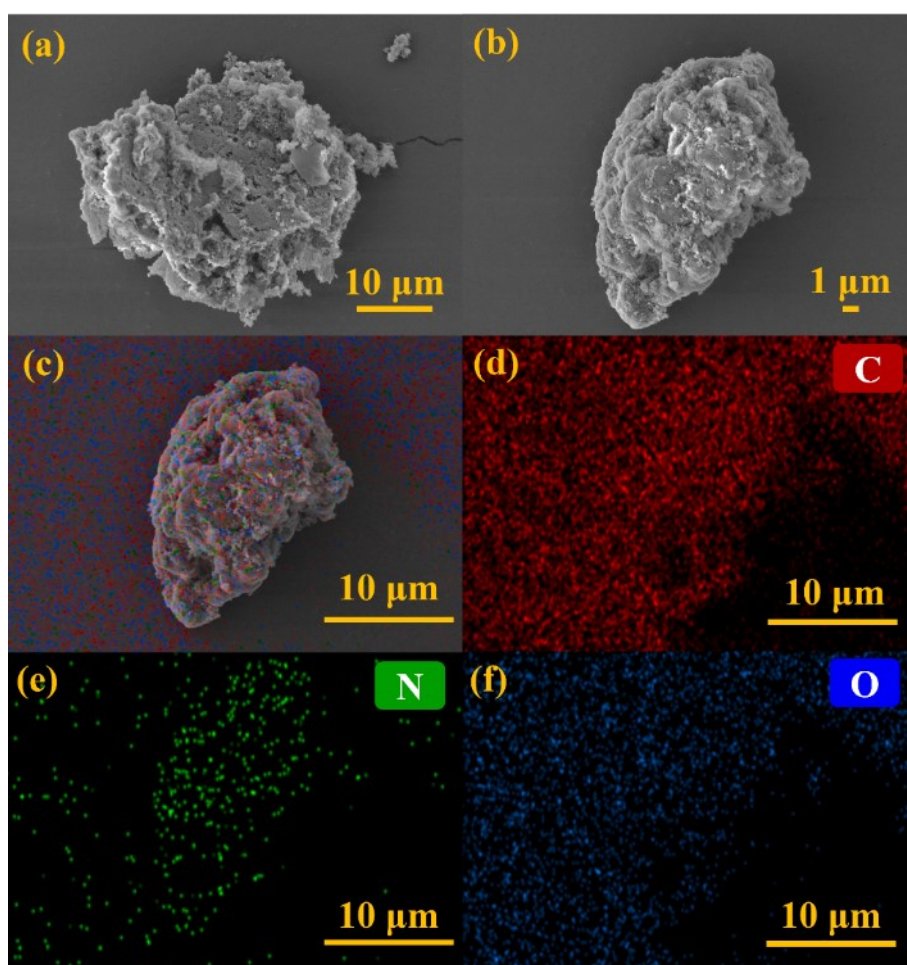


**Figure S21.** (a, b) SEM images of Tp-AD-1 and (c, d, e, f) SEM-EDS mapping images of Tp-AD-1.

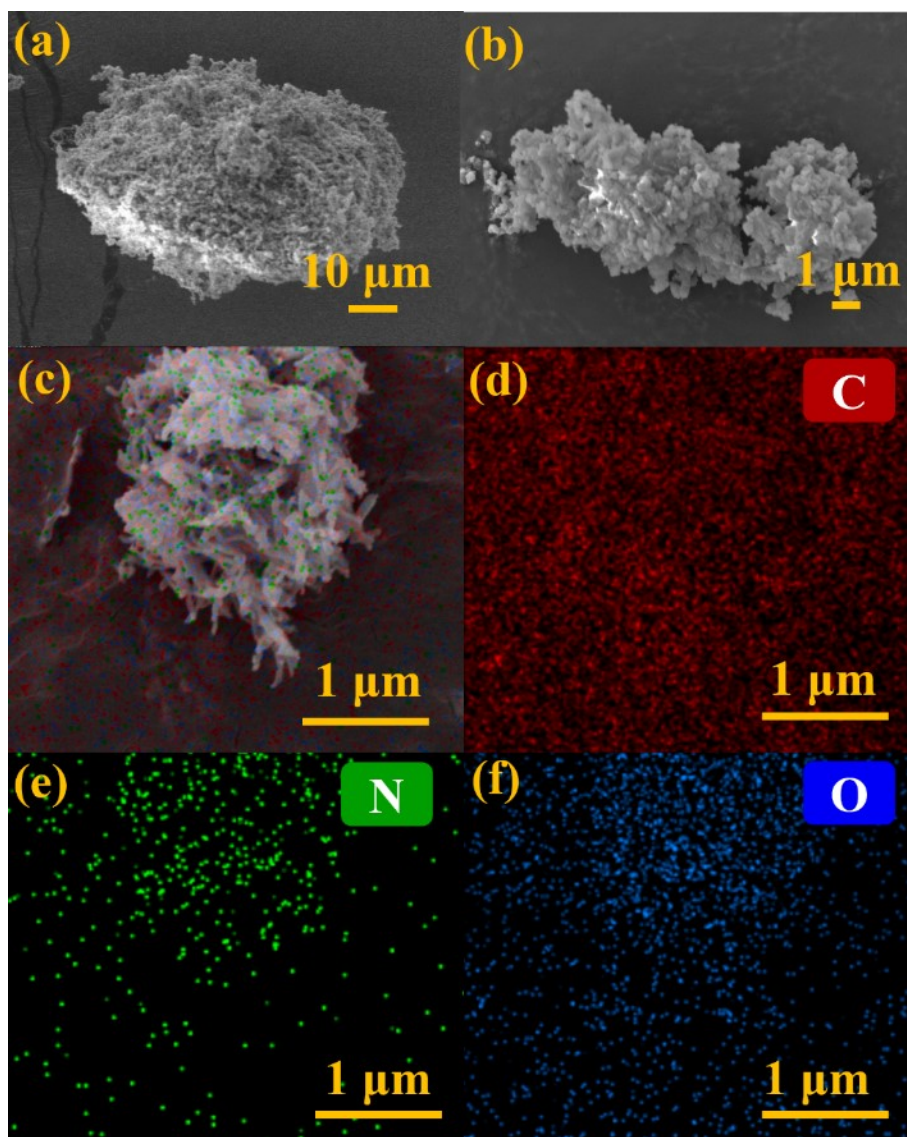


**Figure S22.** (a, b) SEM images of Tp-AD-2 and (c, d, e, f) SEM-EDS mapping images of Tp-AD-2.

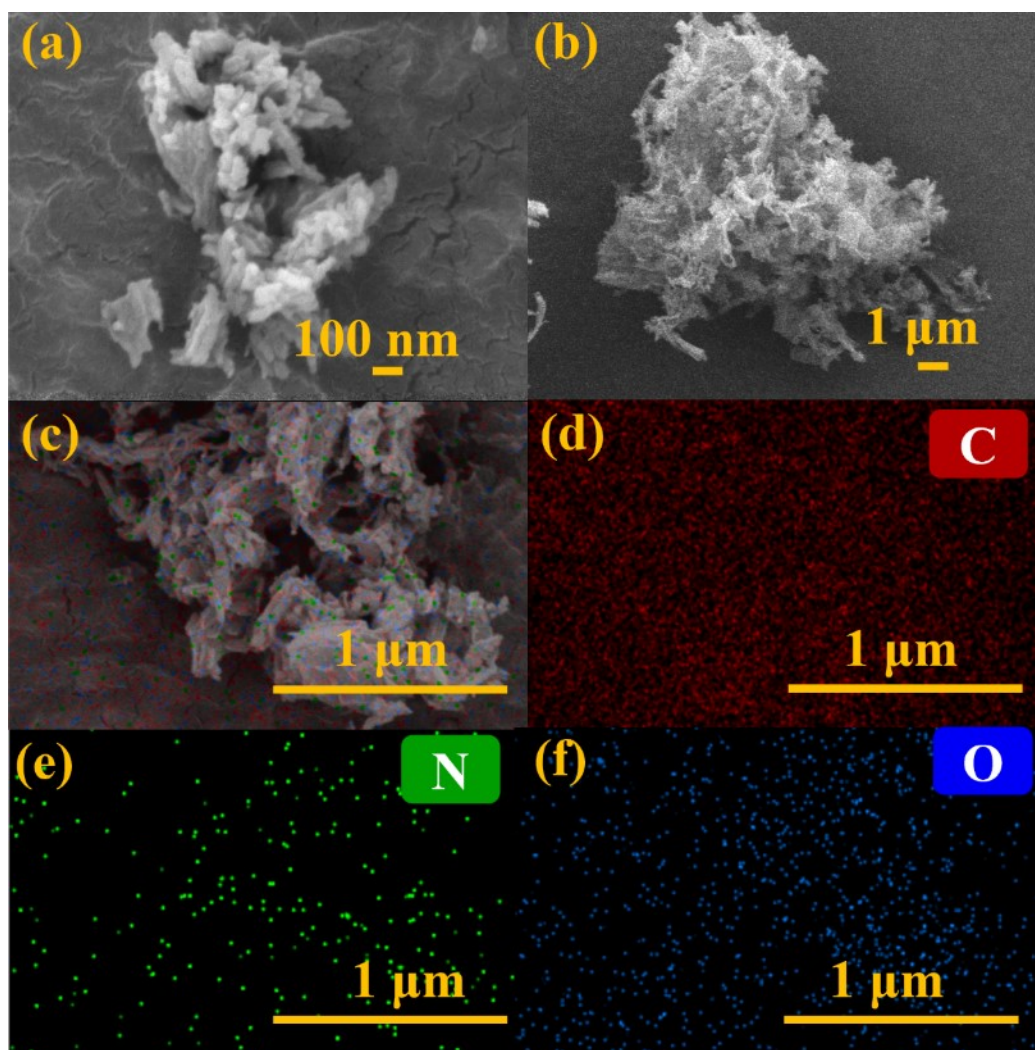


**Figure S23.** (a, b) SEM images of Tp-AD-3 and (c, d, e, f) SEM-EDS mapping images of Tp-AD-3.

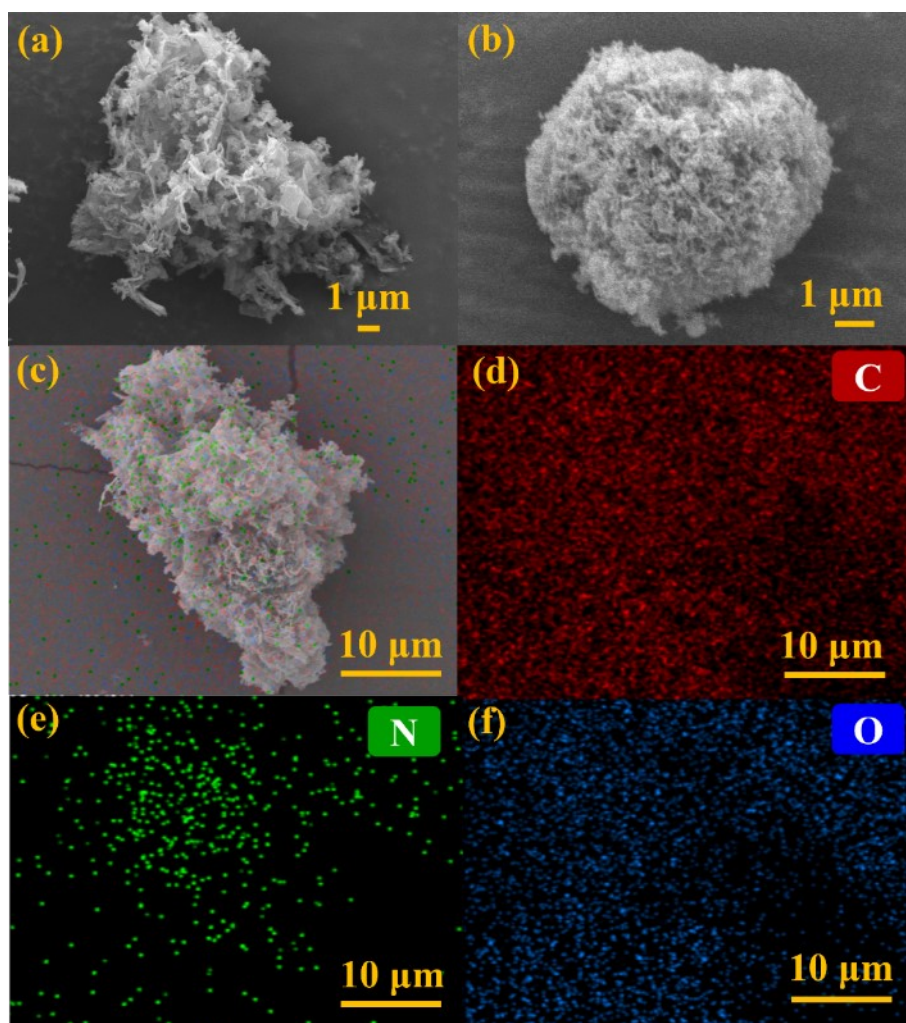


**Figure S24.** (a, b) SEM images of Tp-AD-4 and (c, d, e, f) SEM-EDS mapping images of Tp-AD-4.

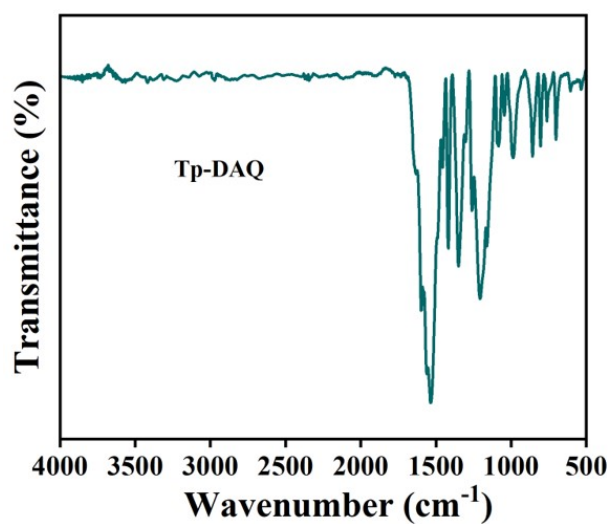


**Figure S25.** FT-IR spectrum of Tp-DAQ.

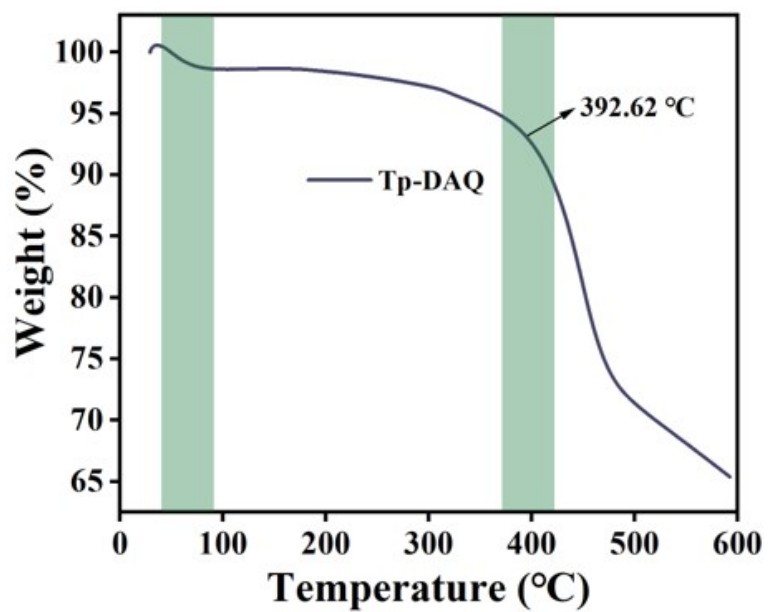


Figure S26. Thermogravimetric analysis (TGA) curves of Tp-DAQ.

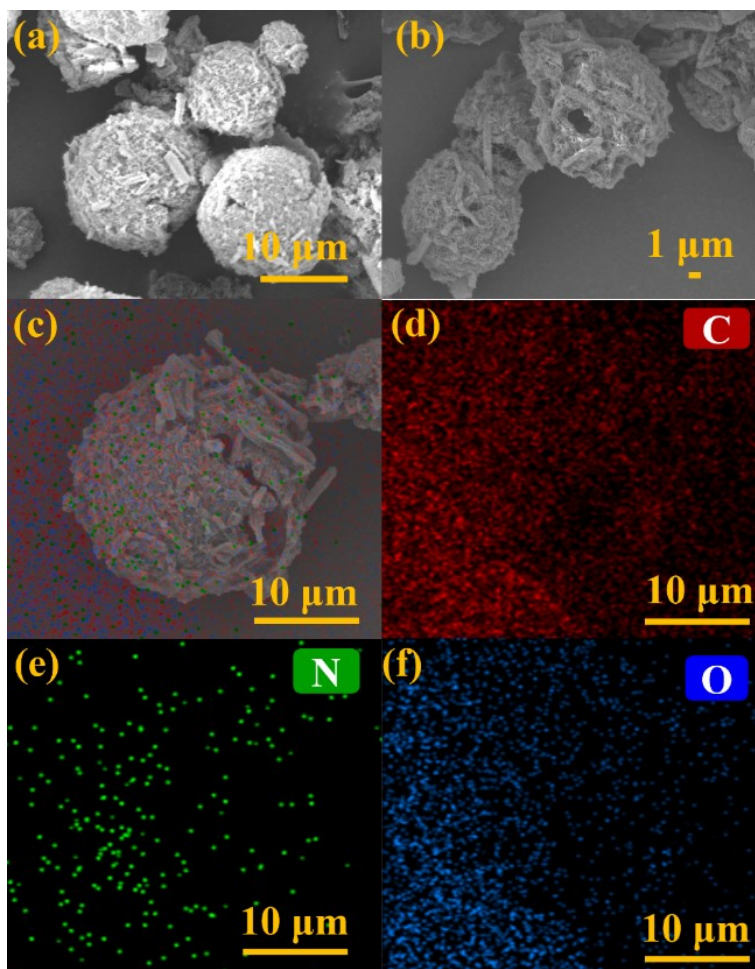
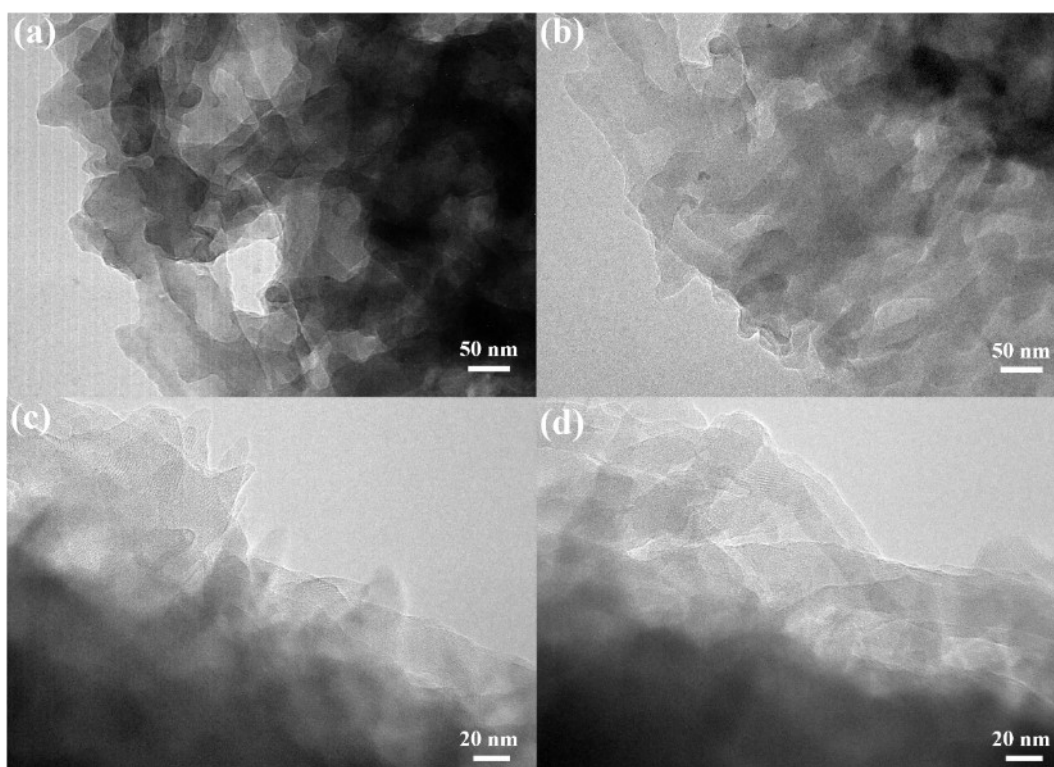
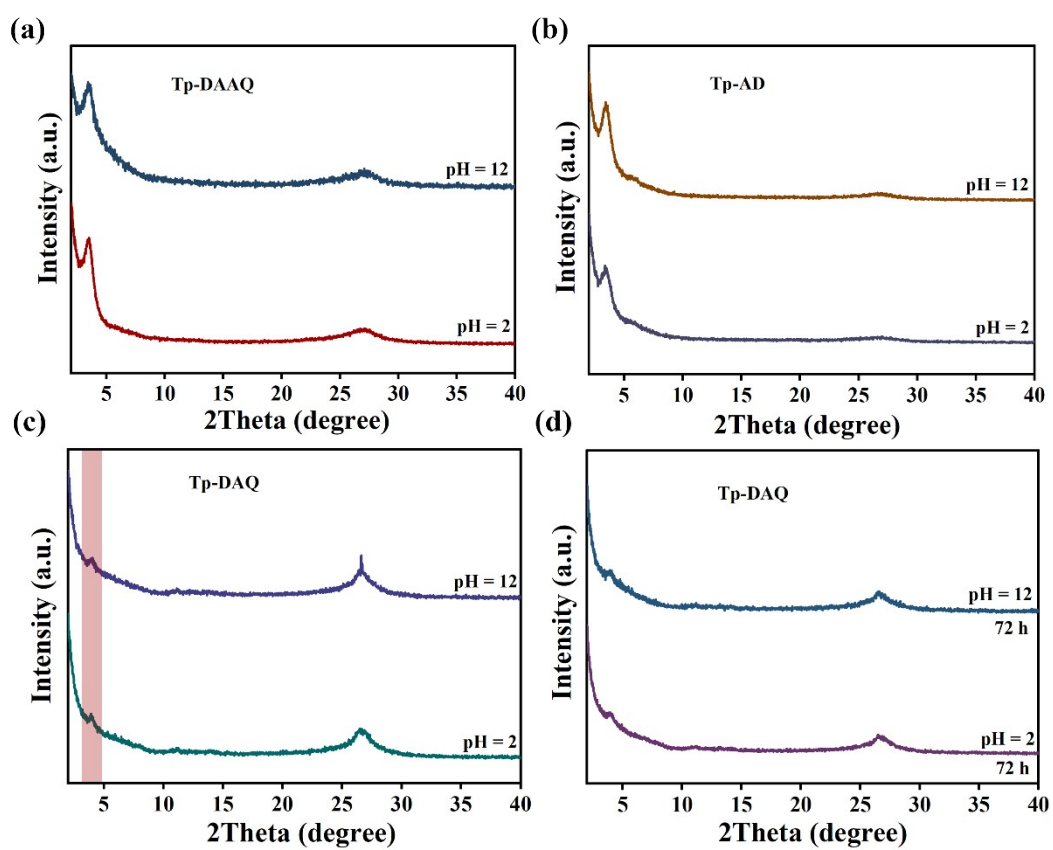


Figure S27. (a, b) SEM images of Tp-DAQ and (c, d, e, f) SEM-EDS mapping images of Tp-DAQ.



**Figure S28.** TEM images of Tp-DAQ.



**Figure S29.** PXRD patterns of (a) Tp-DAAQ, (b) Tp-AD and (c) Tp-DAQ after being immersed in different pH solutions for 24 h and (d) PXRD pattern of Tp-DAQ after being immersed in different pH solutions for 72 h.

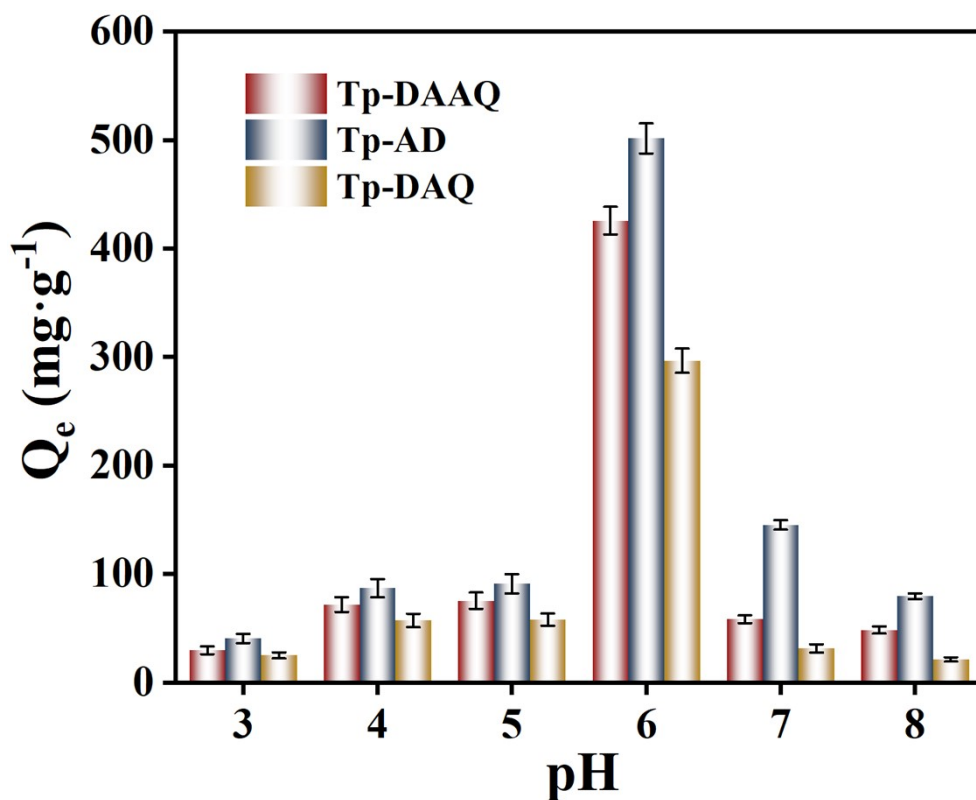


**Figure S30.** Effect of pH for the uranium adsorption on Tp-DAAQ, Tp-AD and Tp-DAQ ( $C_0 = 100$  ppm and  $m/V = 1/10$  g·L<sup>-1</sup>).

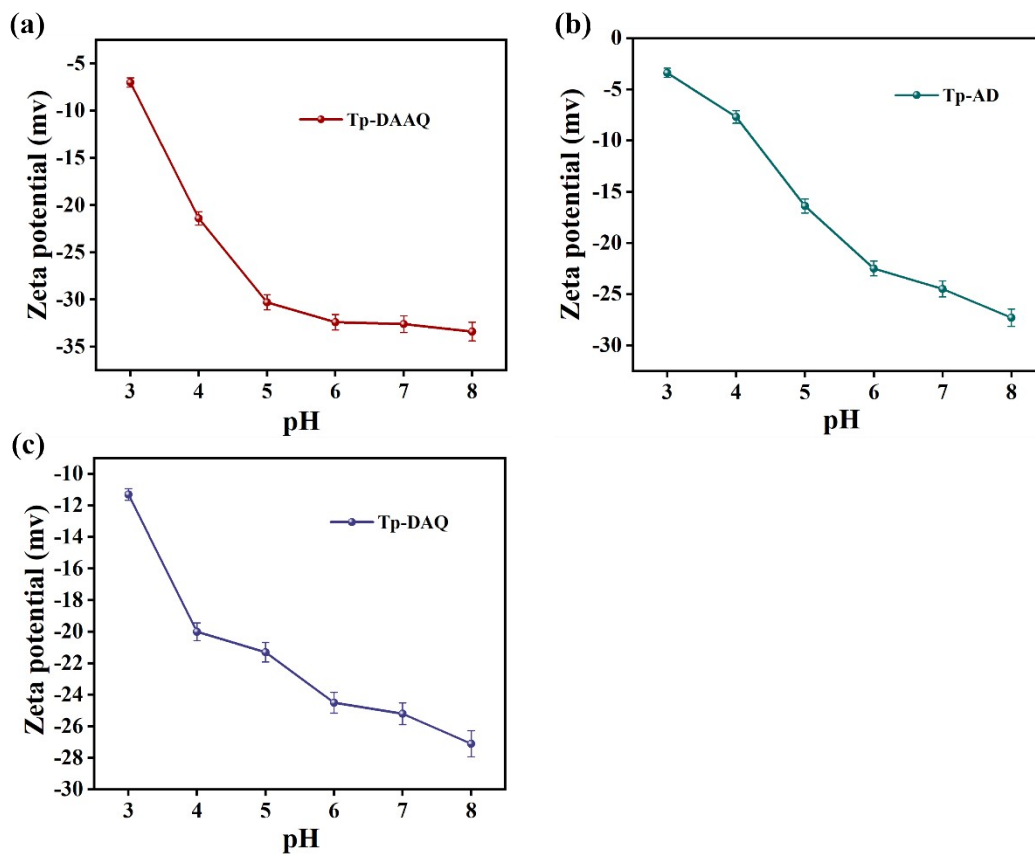


**Figure S31.** Zeta potential of (a) Tp-DAAQ, (b) Tp-AD and (c) Tp-DAQ at the pH range of 3-8.

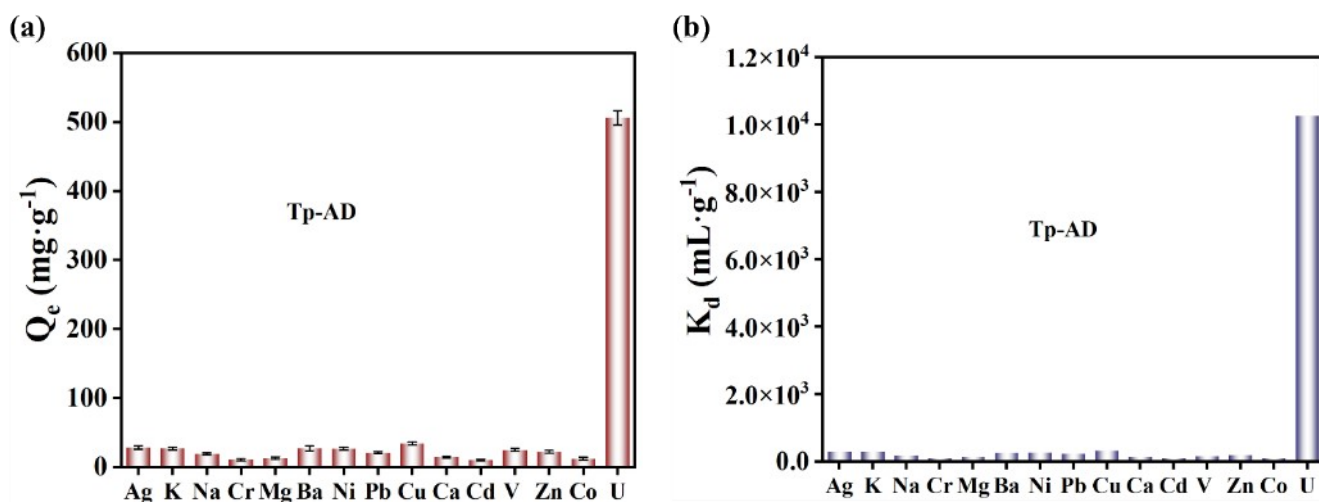


**Figure S32.** (a) Adsorption selectivity study of Tp-AD for gold ( $C_{\text{single metal ion}} = 100 \text{ mg}\cdot\text{L}^{-1}$  and  $t = 12 \text{ h}$ ) and (b) comparison of distribution coefficient ( $K_d$ ) of Tp-AD for different metal ions ( $C_0 = 100 \text{ mg}\cdot\text{L}^{-1}$ ,  $\text{pH} = 6$ ,  $\text{m}/\text{V} = 1/10 \text{ g}\cdot\text{L}^{-1}$  and  $t = 12 \text{ h}$ ).

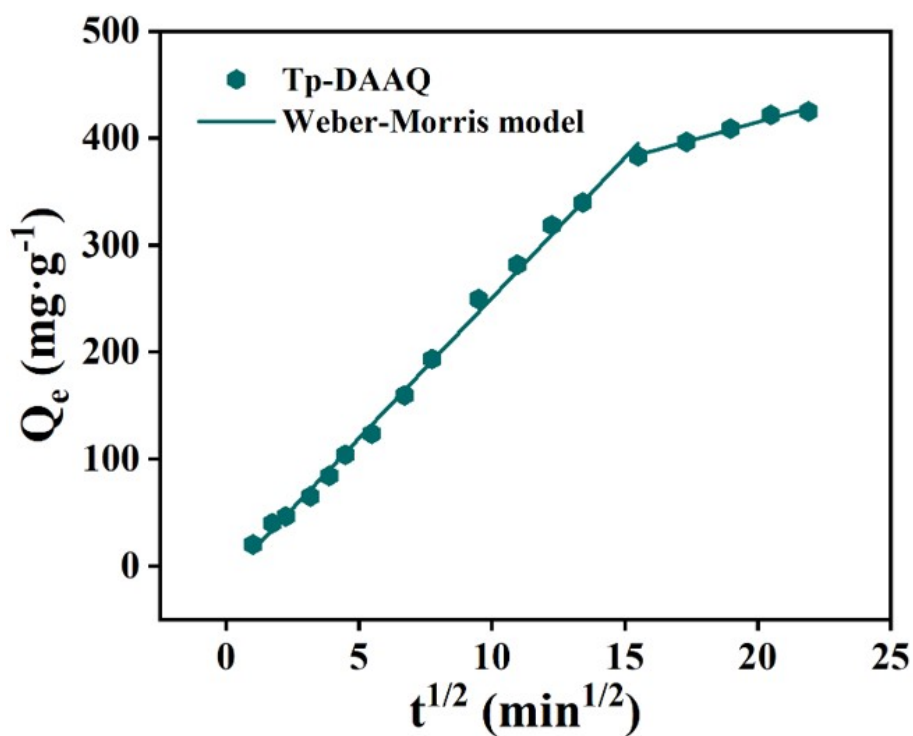


**Figure S33.** Adsorption kinetics curve of Tp-DAAQ fitting with Weber-Morris model.

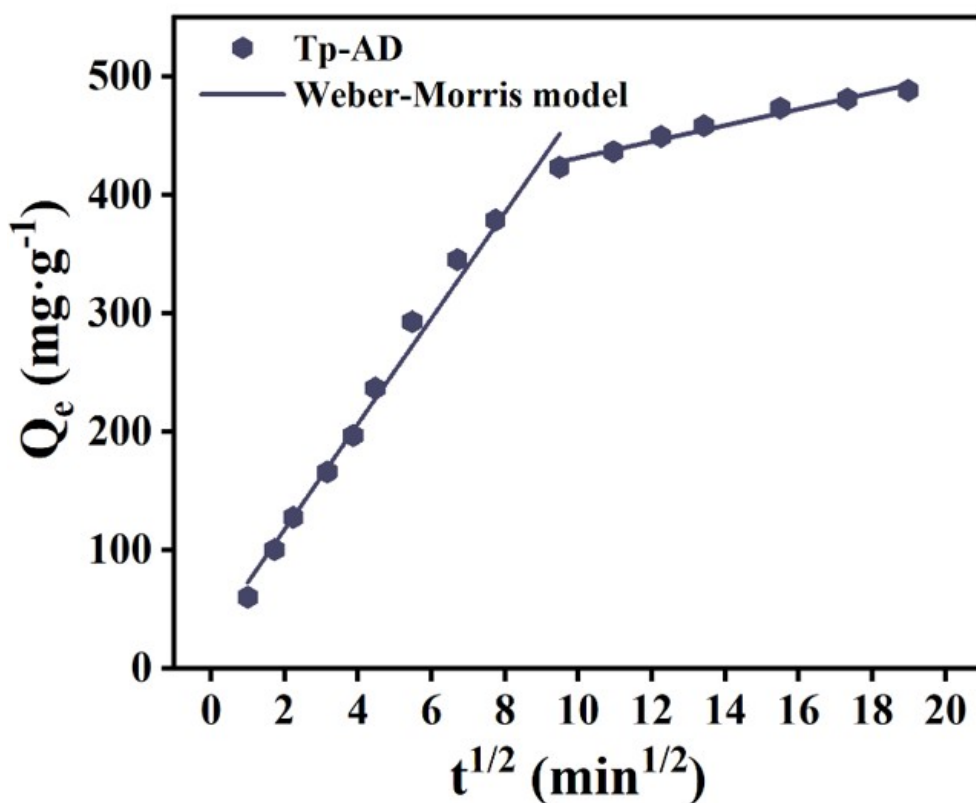


Figure S34. Adsorption kinetics curve of Tp-AD fitting with Weber-Morris model.

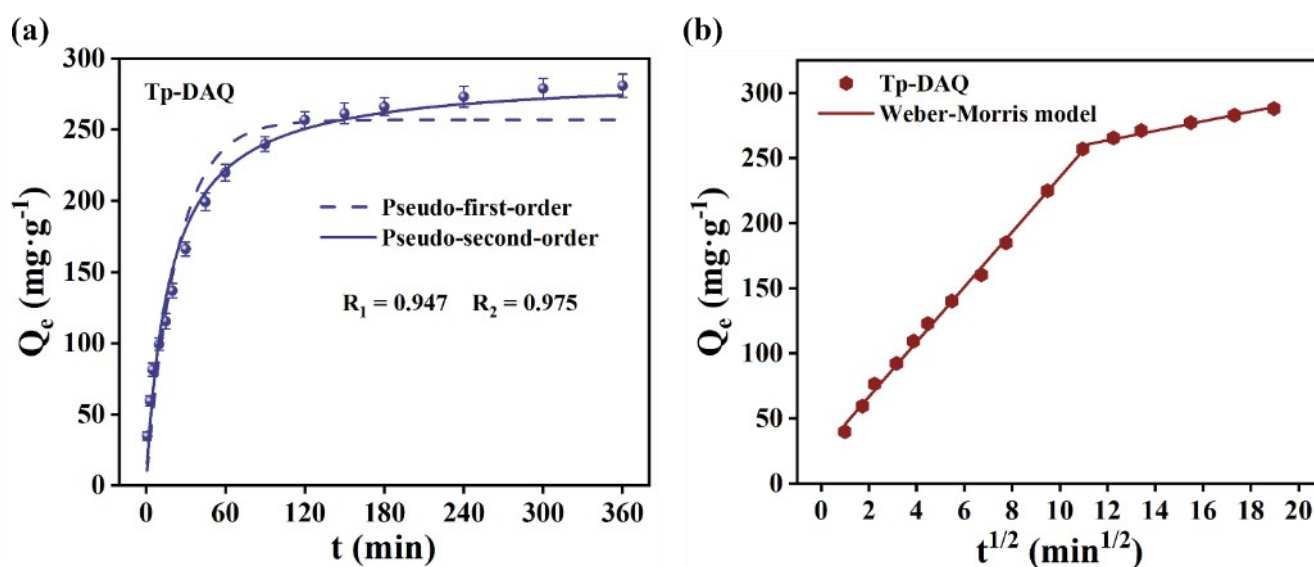


Figure S35. Adsorption kinetics curve of Tp-DAQ fitting with (a) pseudo-first-order and pseudo-second-order models and (b) Weber-Morris model.

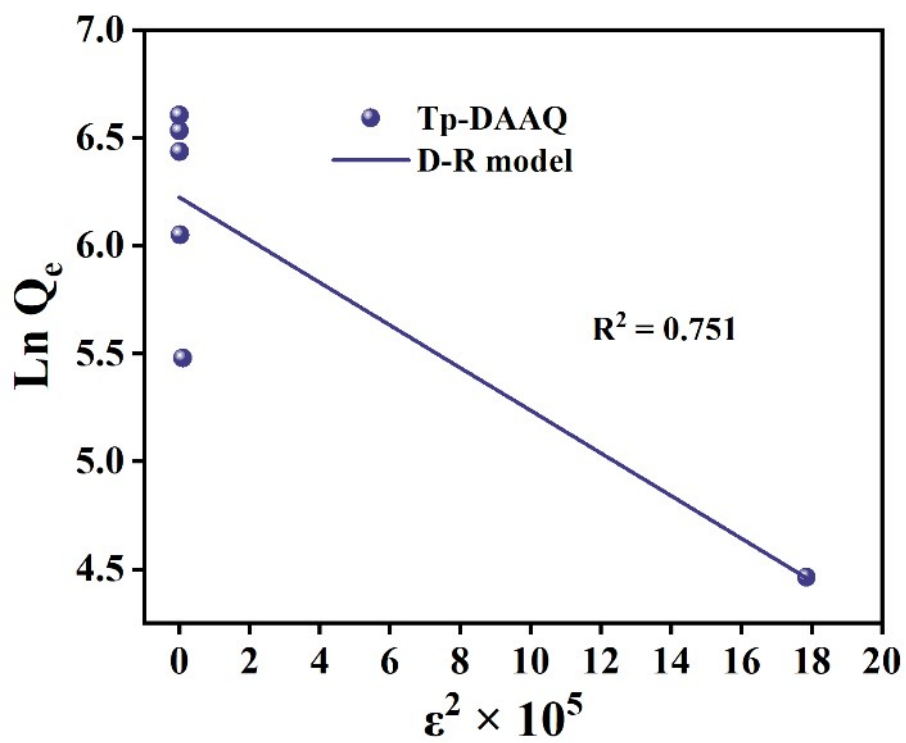


Figure S36. Adsorption isotherm curve of Tp-DAAQ fitting with D-R model.

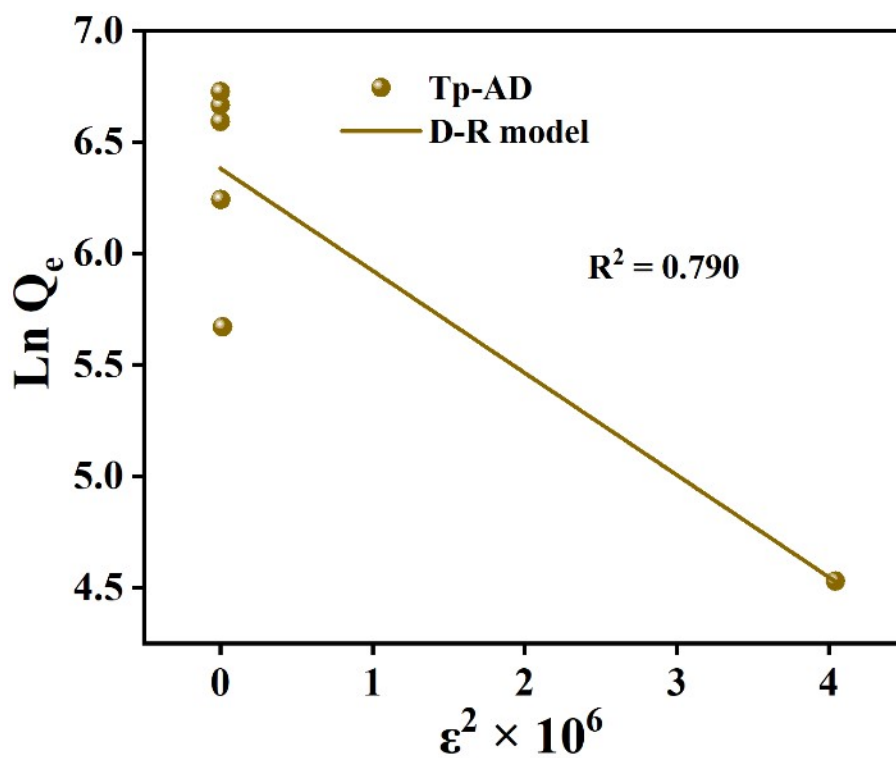
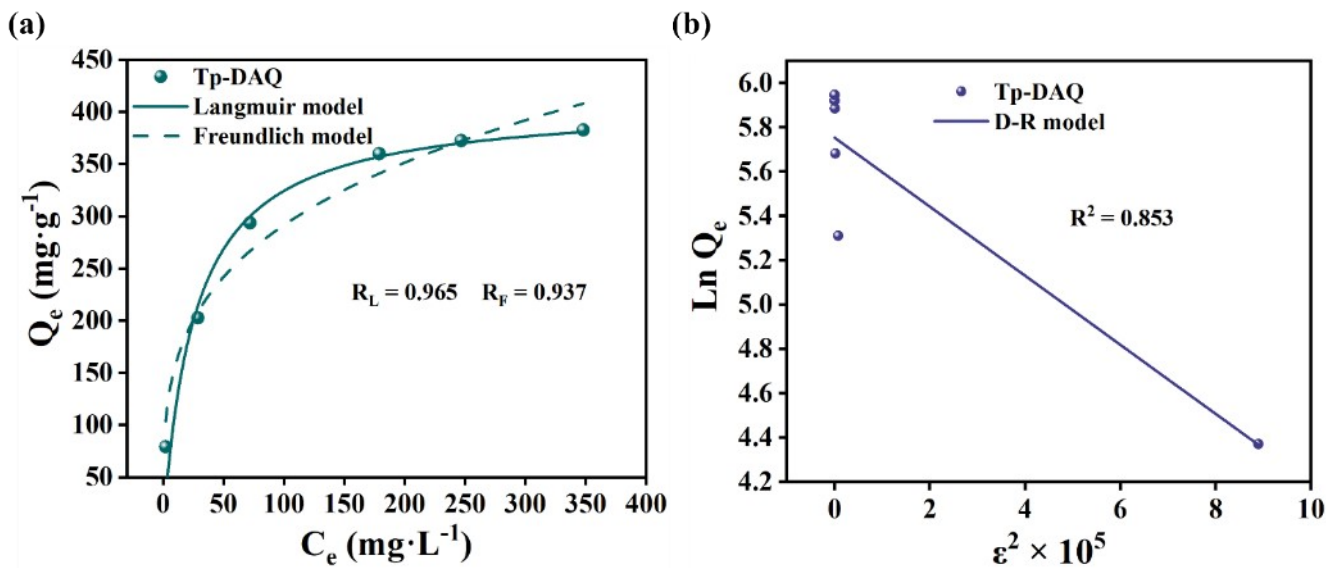
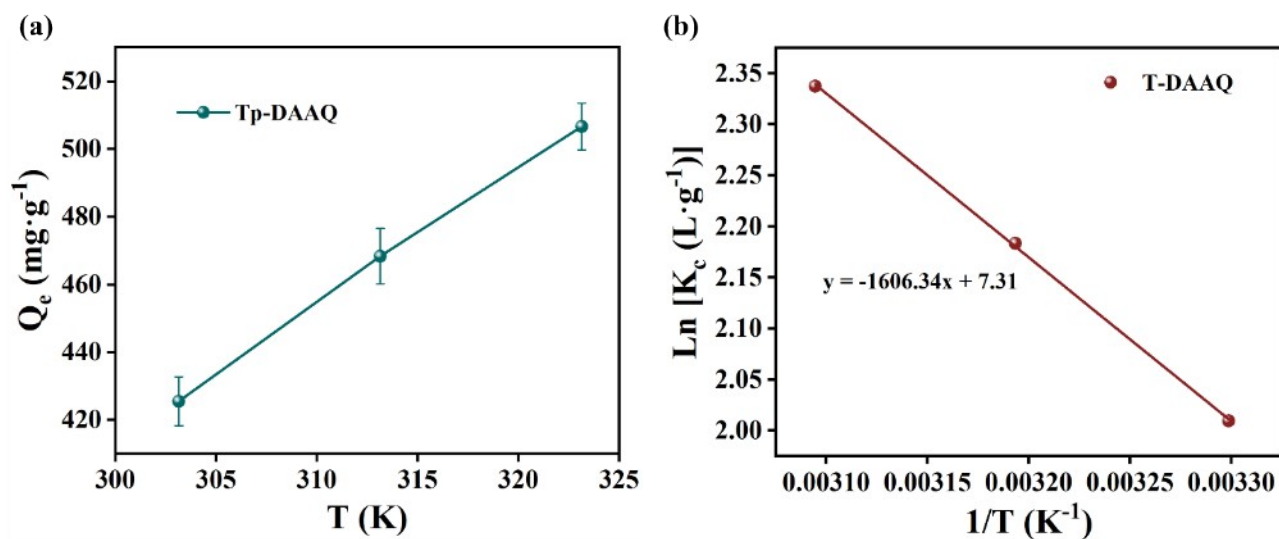


Figure S37. Adsorption isotherm curve of Tp-AD fitting with D-R model.



**Figure S38.** Adsorption isotherm curve of Tp-DAQ fitting with (a) Langmuir model as well as Freundlich model and (b) D-R model.



**Figure S39.** (a) The relation between temperature and adsorption capacity of Tp-DAAQ for uranium; (b) linear curve of  $\ln K_c$  vs  $1/T$ .

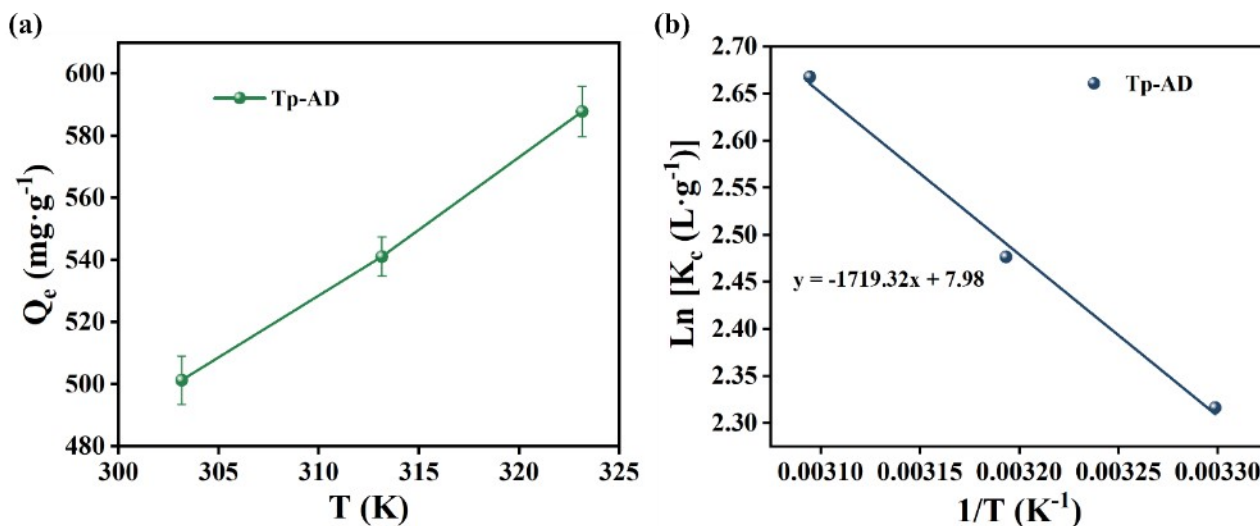


**Figure S40.** (a) The relation between temperature and adsorption capacity of Tp-AD for uranium; (b) linear curve of  $\ln K_c$  vs  $1/T$ .

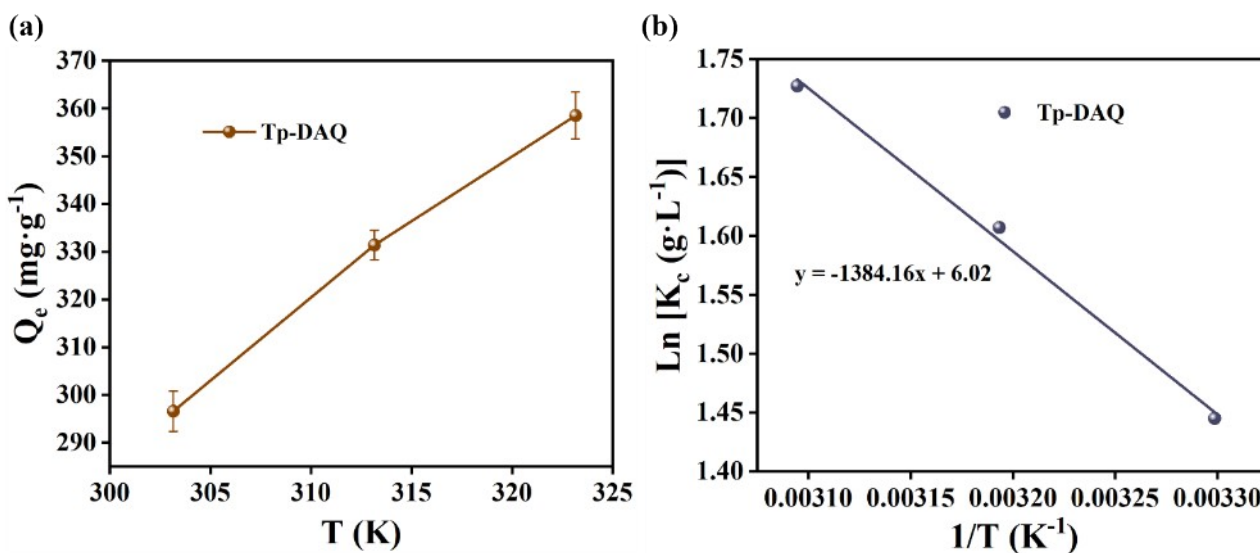


**Figure S41.** (a) The relation between temperature and adsorption capacity of Tp-DAQ for uranium; (b) linear curve of  $\ln K_c$  vs  $1/T$ .

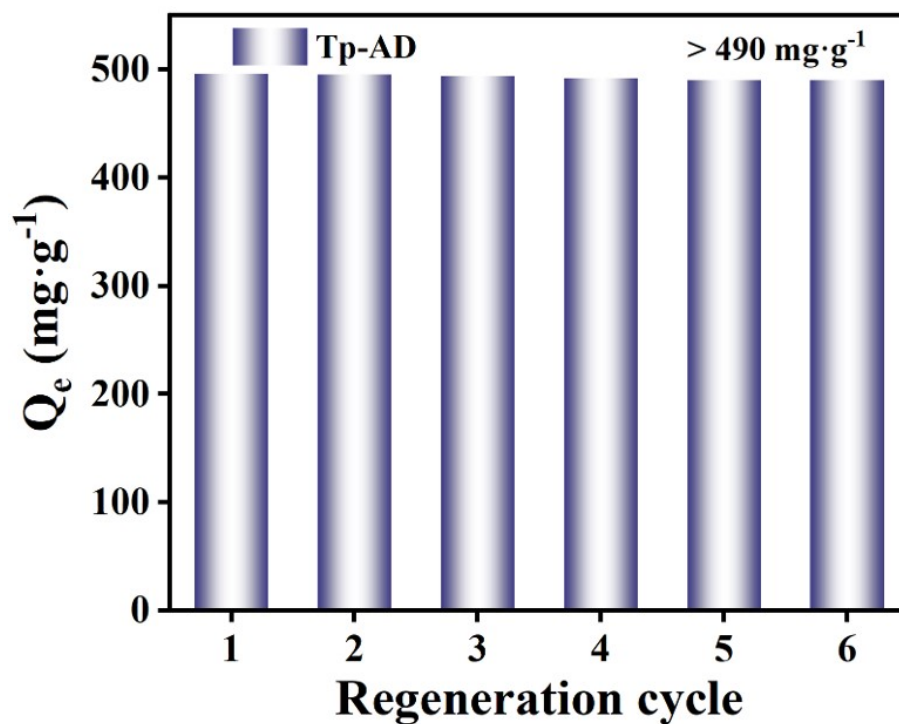


**Figure S42.** The regeneration cycle of Tp-AD for uranium capture ( $C_0 = 100 \text{ mg}\cdot\text{L}^{-1}$ ,  $\text{pH} = 6$ ,  $m/V = 1/10 \text{ g}\cdot\text{L}^{-1}$  and  $t = 8 \text{ h}$ ).

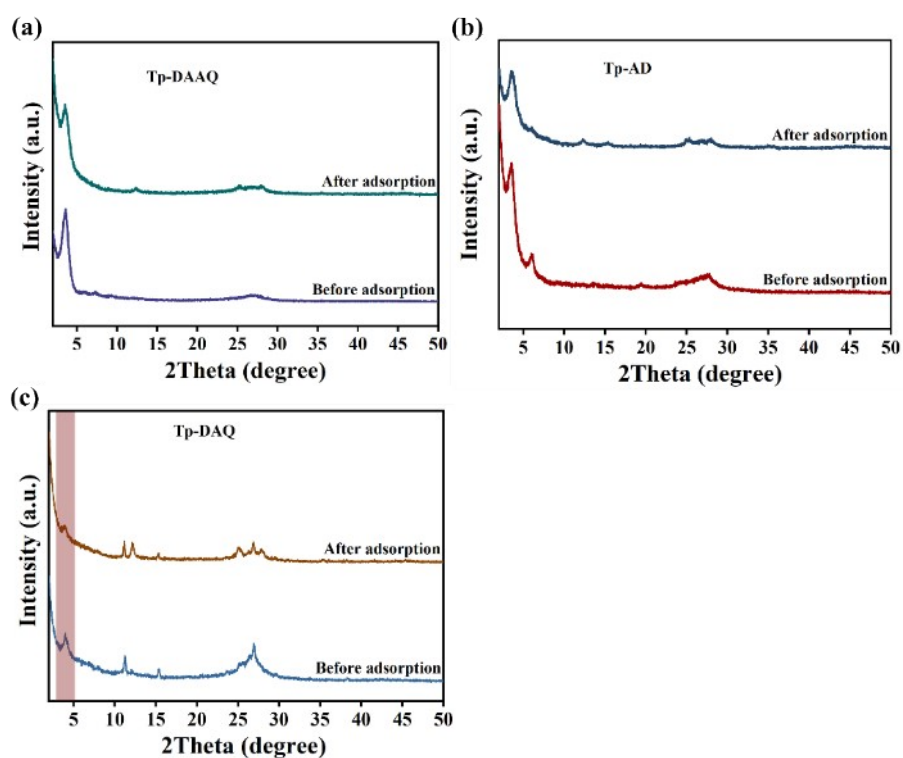


**Figure S43.** PXRD patterns of (a) Tp-DAAQ, (b) Tp-AD and (c) Tp-DAQ before and after uranium adsorption.

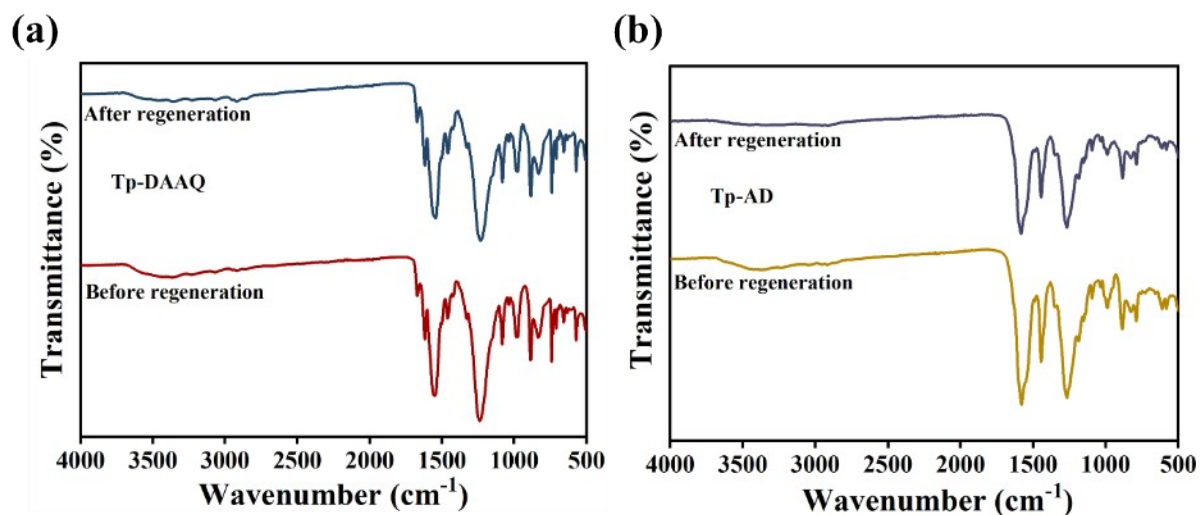


Figure S44. FT-IR spectra of (a) Tp-DAAQ and (b) Tp-AD before and after regeneration.

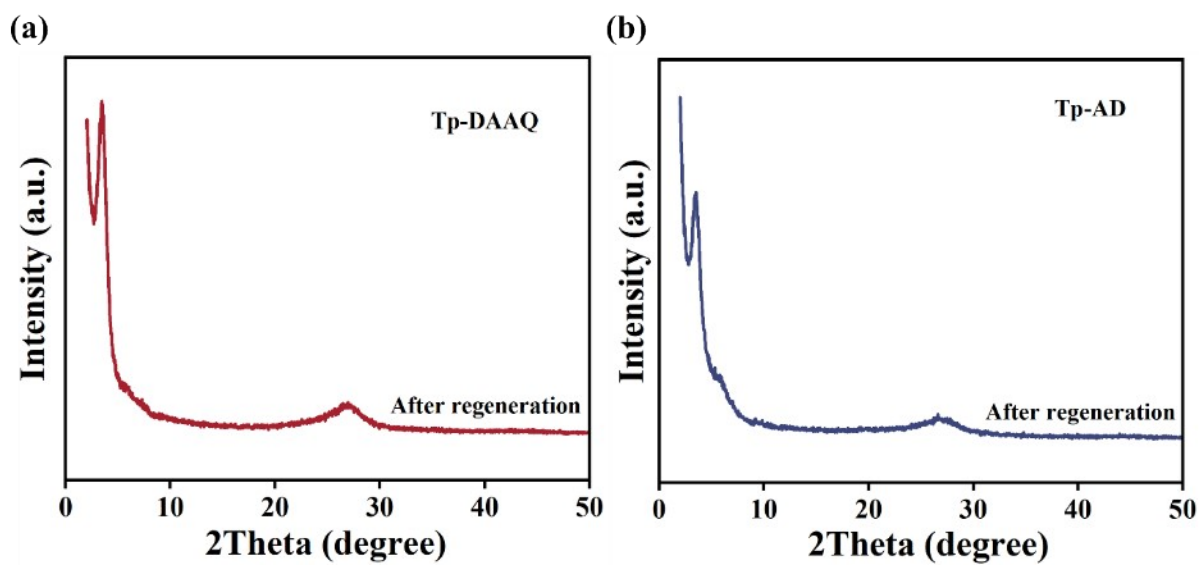
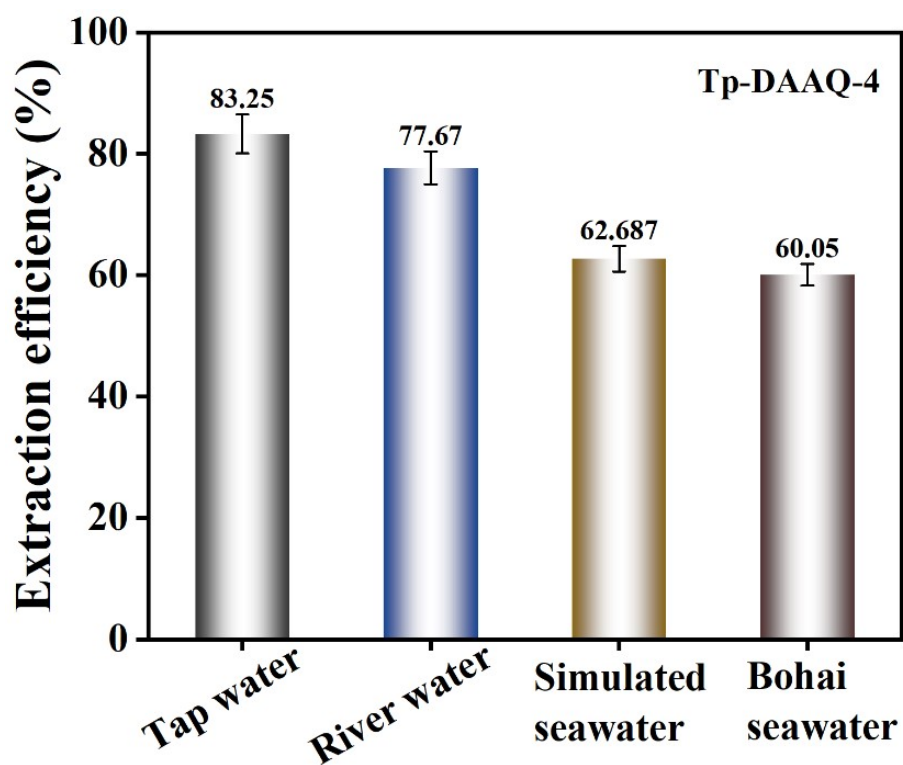
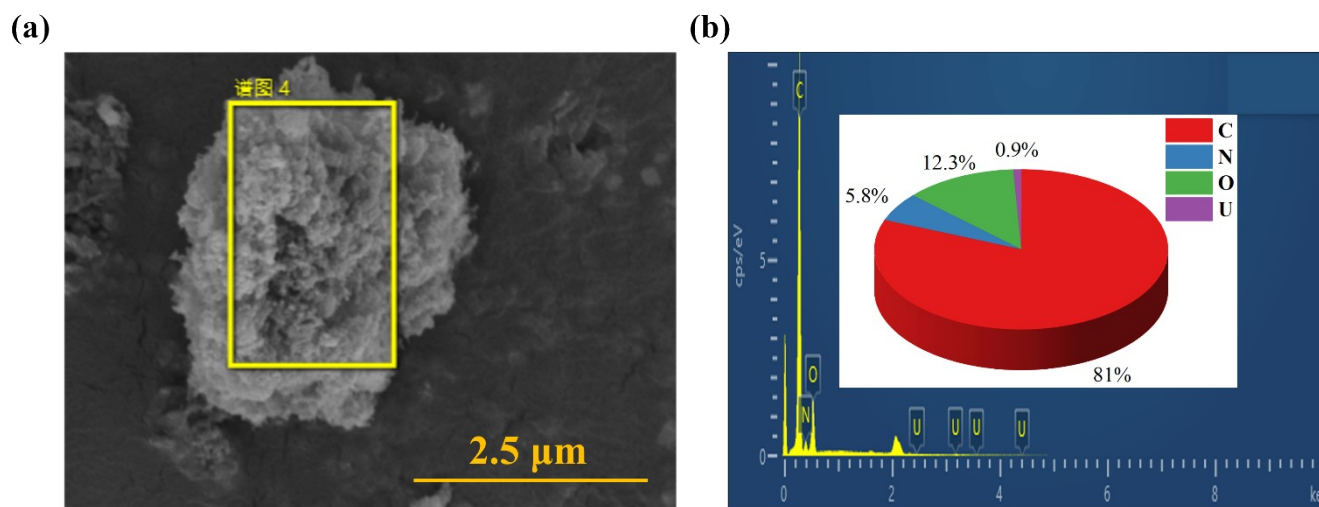


Figure S45. PXRD patterns of (a) Tp-DAAQ and (b) Tp-AD before and after regeneration.



**Figure S46.** The extraction efficiency of Tp-DAAQ-4 for uranium in actual water environments.



**Figure S47.** (a) SEM images and (b) SEM-EDS of Tp-DAAQ-U.

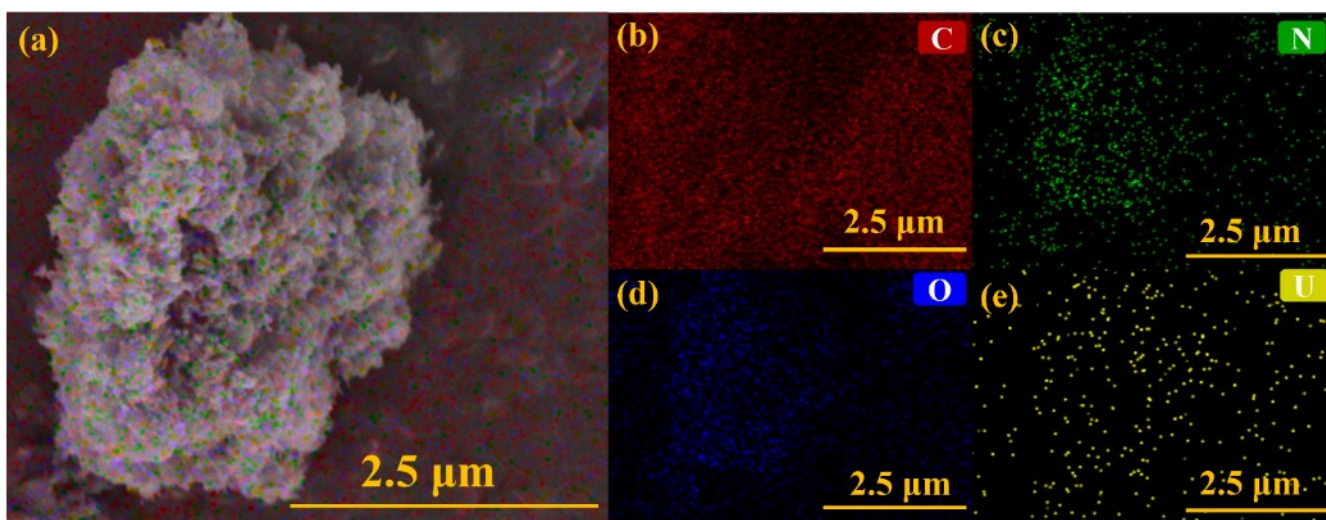


Figure S48. (a, b, c, d, e) SEM-EDS mapping of Tp-DAAQ-U.

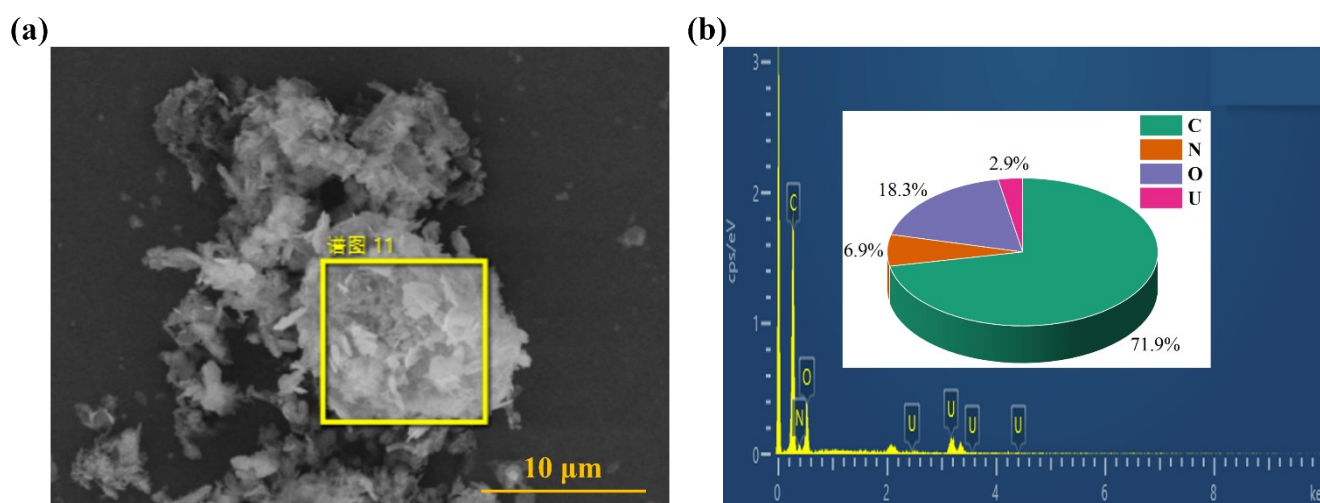


Figure S49. (a) SEM images and (b) SEM-EDS of Tp-AD-U.

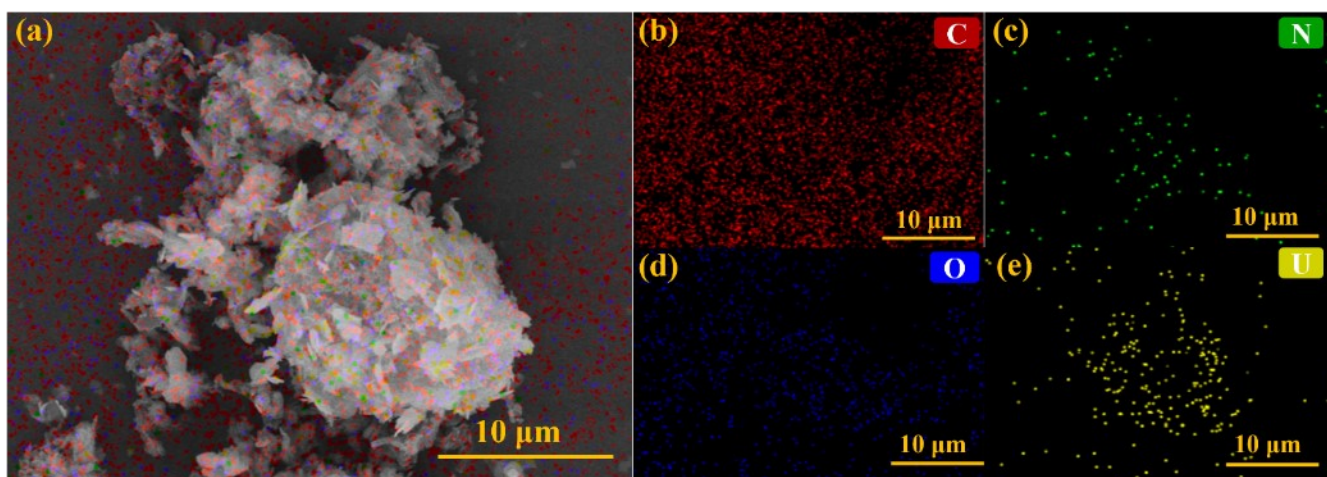


Figure S50. (a, b, c, d, e) SEM-EDS mapping of Tp-AD-U.

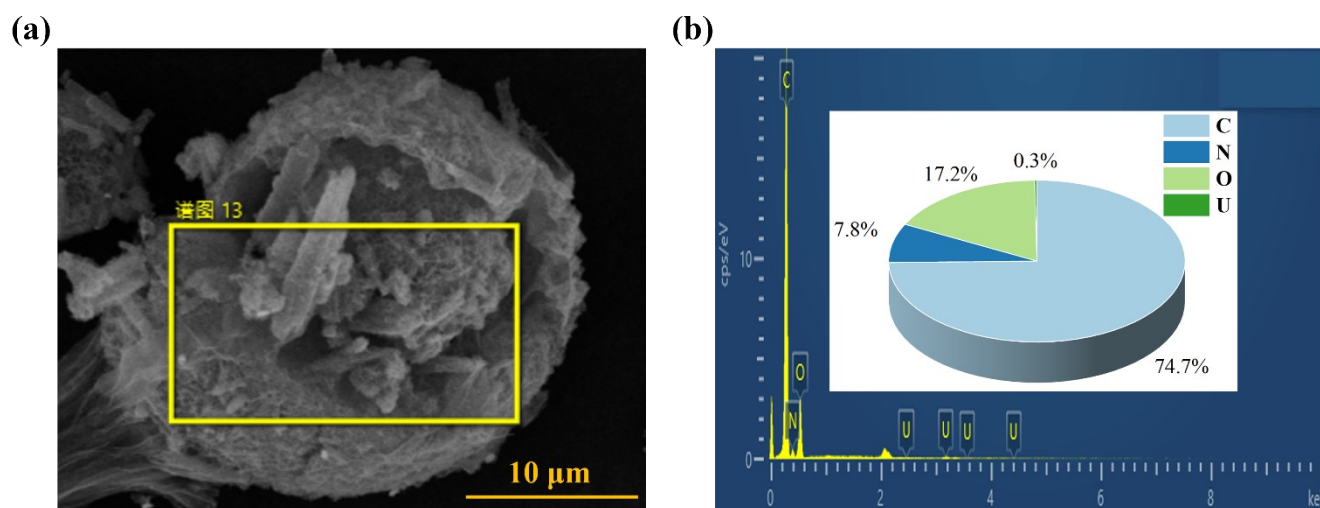
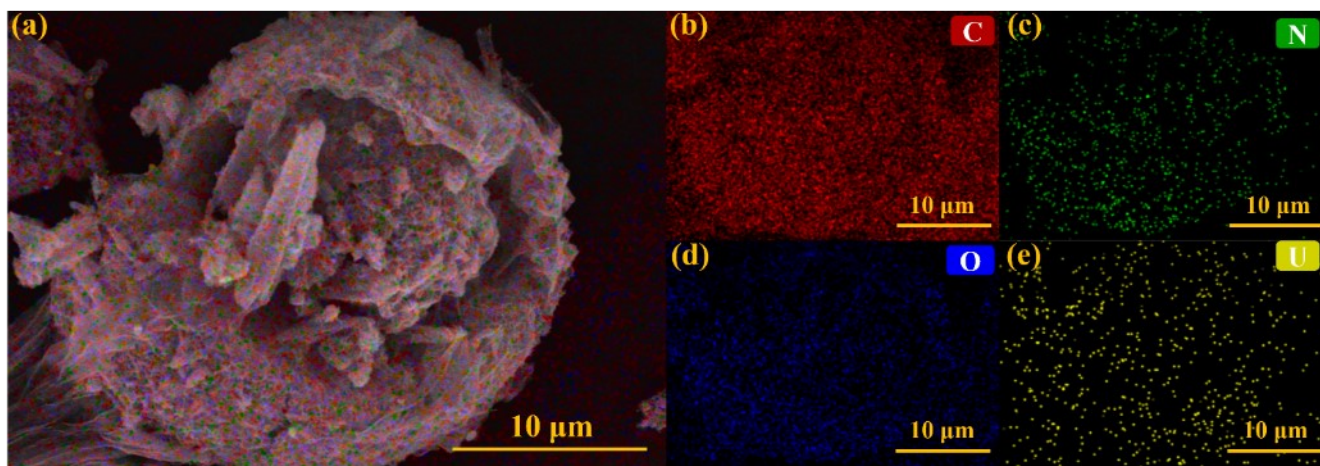
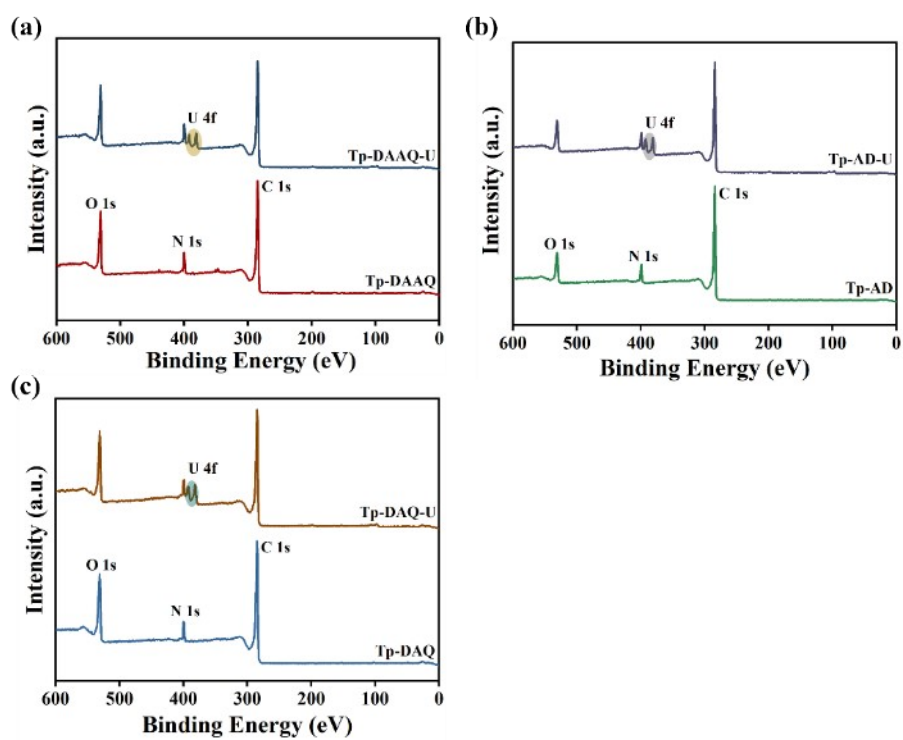


Figure S51. (a) SEM images and (b) SEM-EDS of Tp-DAQ-U.



**Figure S52.** (a, b, c, d, e) SEM-EDS mapping of Tp-DAQ-U.



**Figure S53.** XPS profiles of (a) Tp-DAAQ, (b) Tp-AD and (c) Tp-DAQ before and after uranium adsorption.

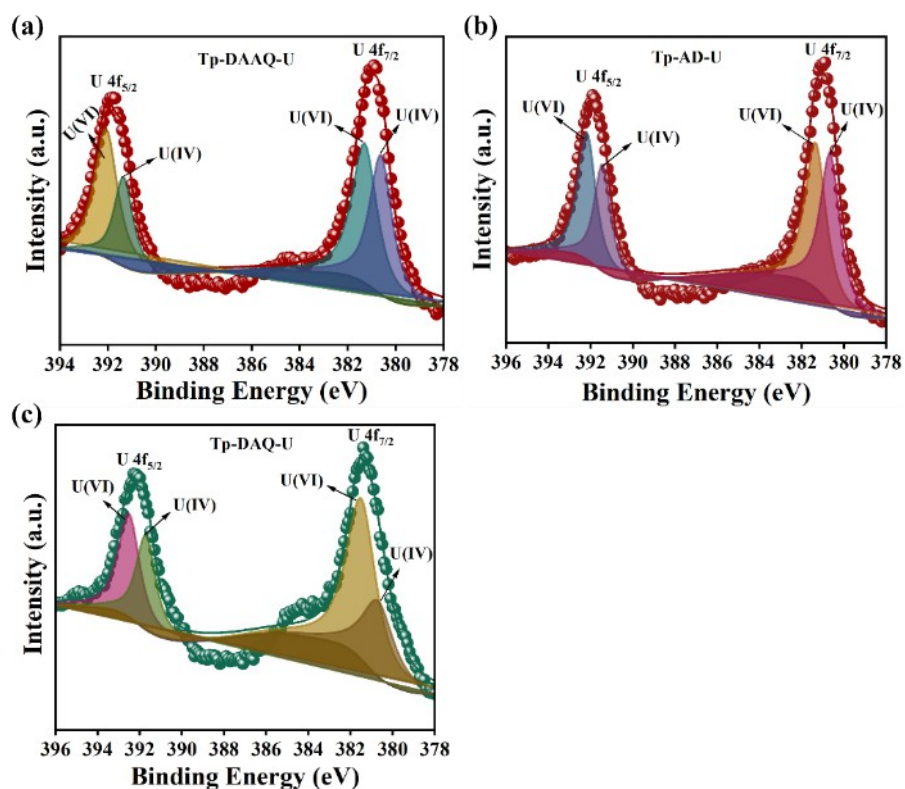


Figure S54. High-resolution U 4f XPS spectra of (a) Tp-DAAQ, (b) Tp-AD and (c) Tp-DAQ after uranium adsorption.

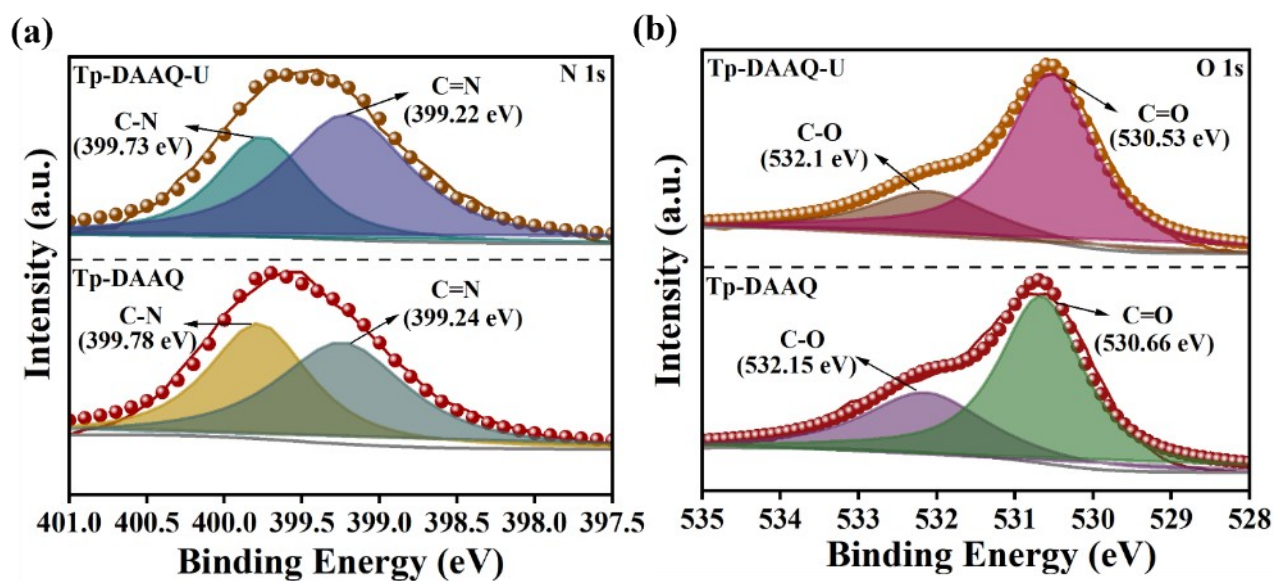


Figure S55. High-resolution (a) N 1s and (b) O 1s XPS spectra of Tp-DAAQ before and after uranium adsorption.

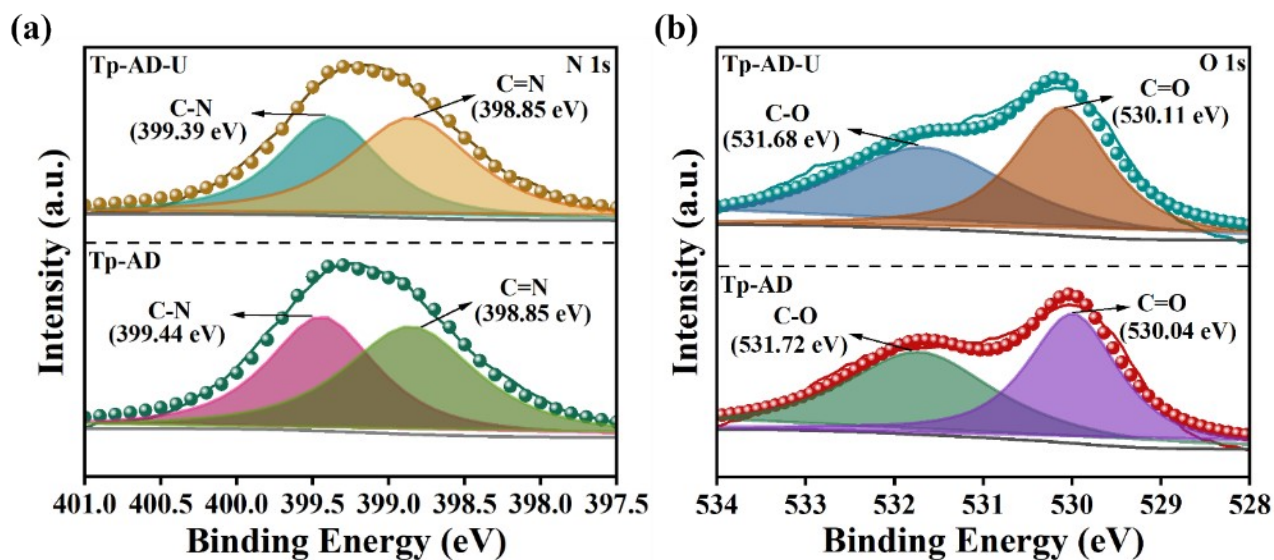


Figure S56. High-resolution (a) N 1s and (b) O 1s XPS spectra of Tp-AD before and after uranium adsorption.

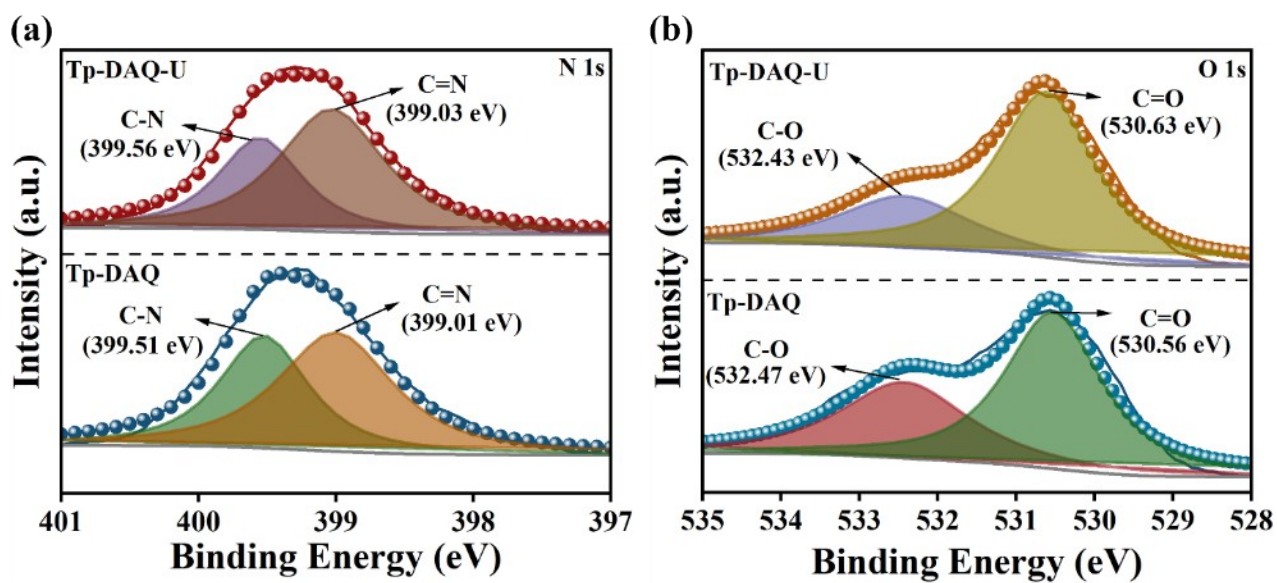
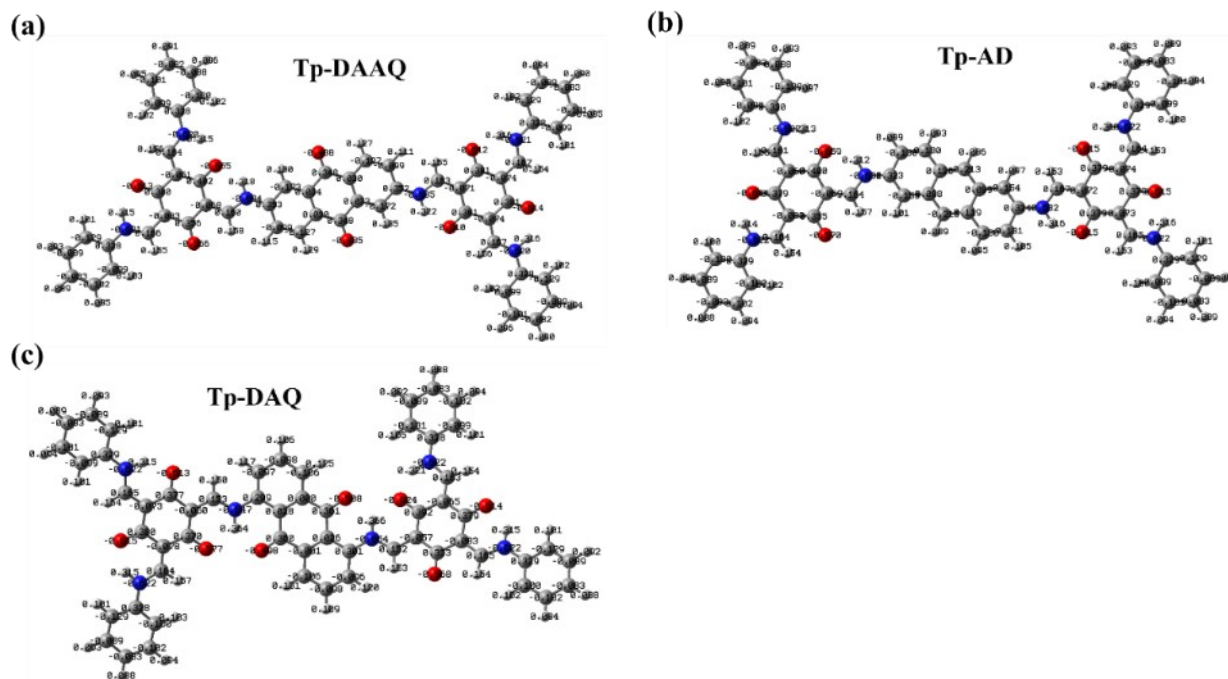
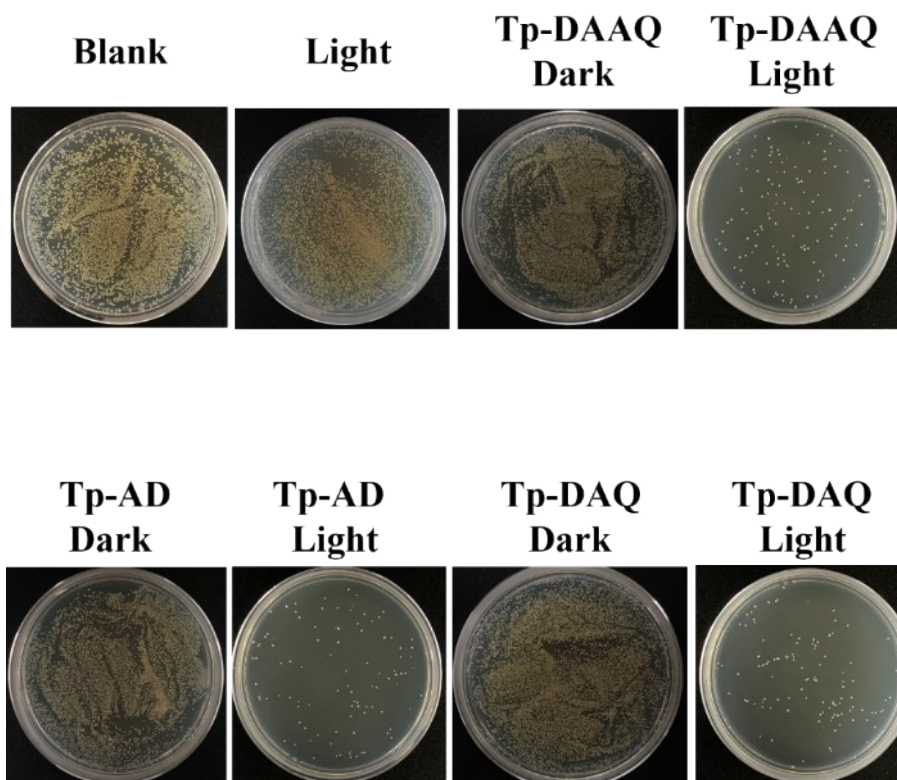


Figure S57. High-resolution (a) N 1s and (b) O 1s XPS spectra of Tp-DAQ before and after uranium adsorption.



**Figure S58.** Mulliken atomic charge distributions of (a) Tp-DAAQ, (b) Tp-AD and (c) Tp-DAQ.



**Figure S59.** Agar plate images of MRSA after incubation with different formulations.

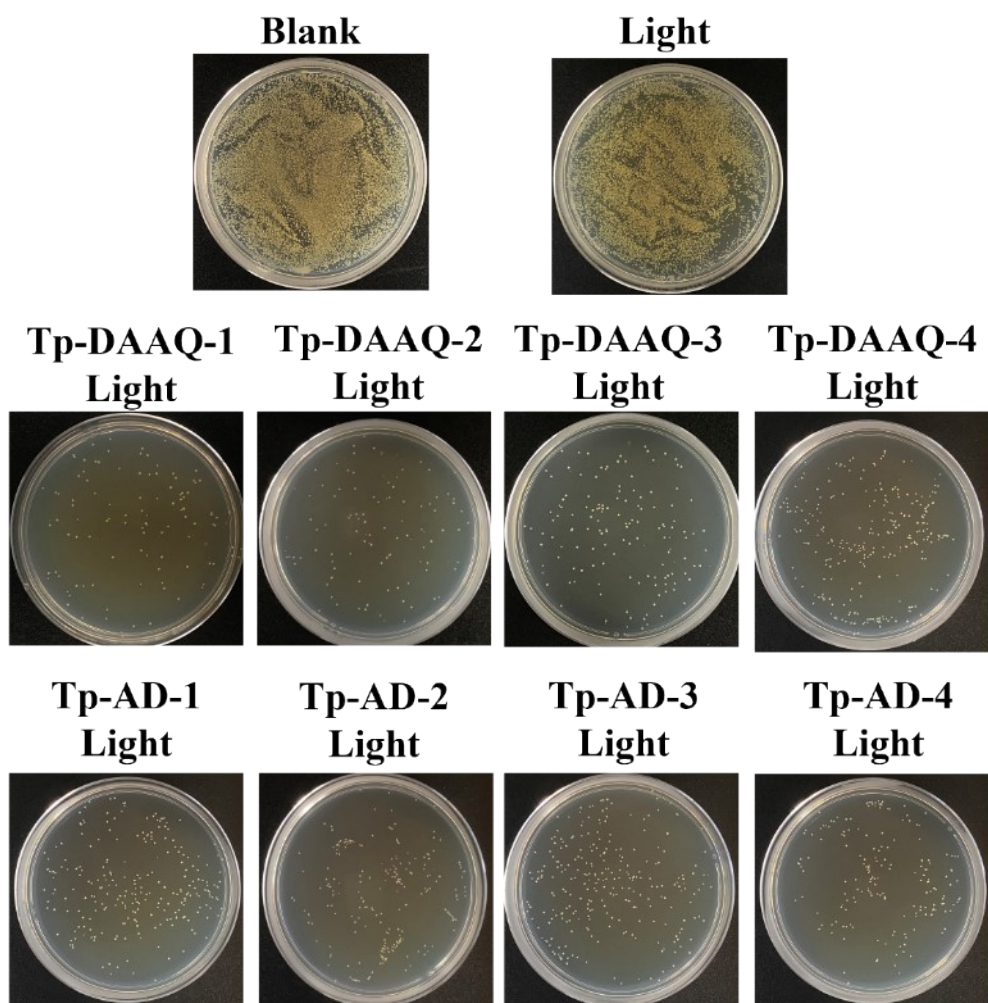


**Figure S60.** Agar plate images of *S. aureus* after incubation with different formulations.

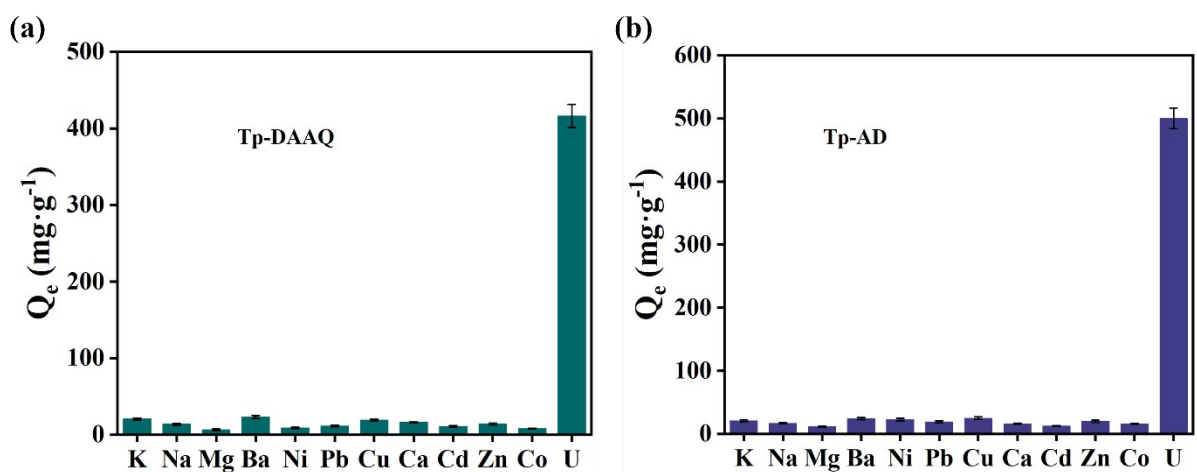


**Figure S61.** Effect of coexisting ions for the uranium extraction on Tp-DAAQ and Tp-AD.

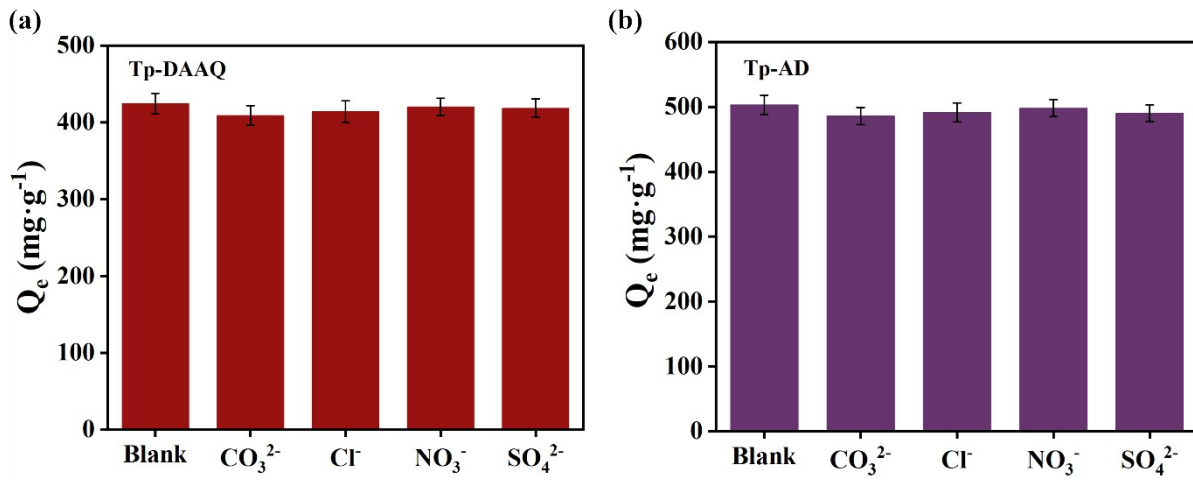


**Figure S62.** Effect of different competing anions for the uranium extraction by Tp-DAAQ and Tp-AD.

**Table S1.** Fractional atomic coordinates of Tp-DAAQ.

---

Space group: P6/M  
a = 29.7470 Å, b = 29.7470 Å, c = 3.6255 Å  
 $\alpha = \beta = 90^\circ, \gamma = 120^\circ$

---

Atom	x (Å)	y (Å)	z (Å)
C1	0.68514	0.38741	0
C2	0.63116	0.35121	0
C3	0.59480	0.36345	0
N4	0.60177	0.41282	0
C5	0.56241	0.42440	0
C6	0.51201	0.38795	0
C7	0.45124	0.46454	0
C8	0.48811	0.45114	0
C9	0.53850	0.48816	0
C10	0.47546	0.40121	0
C11	0.57498	0.47427	0
O12	0.59513	0.57036	0
O13	0.69962	0.43138	0
H14	0.44564	0.66961	0
H15	0.50322	0.65384	0
H16	0.56602	0.63056	0
H17	0.38922	0.50023	0
H18	0.63702	0.44354	0

---

**Table S2.** Fractional atomic coordinates of Tp-AD.

---

Space group: P63/M  
a = 31.2270 Å, b = 31.2270 Å, c = 3.8087 Å  
 $\alpha = \beta = 90^\circ, \gamma = 120^\circ$

---

Atom	x (Å)	y (Å)	z (Å)
C1	0.35411	0.62079	0
C2	0.38874	0.60914	0
N3	0.3821	0.5621	0
C4	0.4196	0.55107	0
C5	0.46762	0.5858	0
C6	0.5255	0.51284	0
C7	0.49039	0.5256	0
C8	0.44238	0.49034	0
C9	0.50243	0.57317	0
C10	0.40763	0.50357	0
C11	0.36905	0.67173	0
O12	0.41094	0.69984	0
H13	0.31359	0.59047	0
H14	0.5194	0.47862	-0.14981
H15	0.56147	0.5362	0.14981
H16	0.34006	0.68375	0

---

**Table S3.** Fractional atomic coordinates of Tp-DAQ.

Space group: P6/M			
a = 25.2370 Å, b = 25.2370 Å, c = 3.5282 Å			
$\alpha = \beta = 90^\circ, \gamma = 120^\circ$			
Atom	x (Å)	y (Å)	z (Å)
C1	0.71352	0.41934	0
C2	0.64994	0.35415	0
C3	0.58785	0.34549	0
N4	0.57779	0.39929	0
C5	0.4586	0.34868	0
C6	0.40289	0.35476	0
C7	0.47662	0.53771	0
C8	0.47306	0.47422	0
C9	0.53029	0.47036	0
C10	0.41019	0.41705	0
C11	0.52145	0.40538	0
O12	0.65041	0.53958	0
O13	0.71539	0.47209	0
H14	0.54317	0.29356	0
H15	0.6207	0.45022	0
H16	0.45358	0.29766	0
H17	0.35187	0.30877	0
H18	0.36477	0.42205	0

**Table S4.** The atomic percentages of Tp-DAAQ, Tp-AD and Tp-DAQ before and after being immersed with uranium solution determined by XPS.

Sample	C (%)	N (%)	O (%)	U (%)	Total (%)
Tp-DAAQ	75.71	6.59	17.7	0	100
Tp-DAAQ-U	75.67	6.58	17.46	0.29	100
Tp-AD	80.41	7.71	11.88	0	100
Tp-AD-U	79.64	7.17	12.83	0.36	100
Tp-DAQ	74.5	6.46	19.04	0	100
Tp-DAQ-U	74.67	5.8	19.13	0.4	100

**Table S5.** N<sub>2</sub> adsorption/desorption data of Tp-DAAQ, Tp-DAAQ-1, Tp-DAAQ-2, Tp-DAAQ-3, Tp-DAAQ-4, Tp-AD, Tp-AD-1, Tp-AD-2, Tp-AD-3, Tp-AD-4 and Tp-DAQ.

Sample	BET specific surface area (m <sup>2</sup> /g)	Pore volume(cm <sup>3</sup> ·g <sup>-1</sup> )
Tp-DAAQ-1	483.05	0.59
Tp-DAAQ-2	502.51	0.62
Tp-DAAQ	789.09	0.84
Tp-DAAQ-3	625.14	0.66
Tp-DAAQ-4	665.84	0.77
Tp-AD-1	108.71	0.45
Tp-AD-2	166.71	0.49
Tp-AD	609.06	0.60
Tp-AD-3	349.85	0.51
Tp-AD-4	417.23	0.53
Tp-DAQ	103.13	0.13

**Table S6.** Uranium adsorption kinetic models onto Tp-DAAQ, Tp-AD and Tp-DAQ.

Kinetics model	Pseudo-first-order			Pseudo-second-order		
	q <sub>e</sub>	K <sub>1</sub>	R <sup>2</sup>	Q <sub>e</sub>	K <sub>2</sub>	R <sup>2</sup>
Tp-DAAQ	400.77	0.01178	0.975	498.90	0.0000233	0.984
Tp-AD	441.70	0.04203	0.955	505.32	0.0000998	0.981
Tp-DAQ	256.98	0.04269	0.947	287.98	0.000194	0.975

**Table S7.** Uranium adsorption isotherm models onto Tp-DAAQ, Tp-AD and Tp-DAQ.

Kinetics model	Langmuir model			Freundlich model		
	q <sub>m</sub>	K <sub>L</sub>	R <sup>2</sup>	K <sub>F</sub>	n	R <sup>2</sup>
Tp-DAAQ	893.80	0.01527	0.986	79.88	2.525	0.953
Tp-AD	952.91	0.02304	0.987	122.21	2.889	0.957
Tp-DAQ	409.41	0.03808	0.965	84.17	3.708	0.937

**Table S8.** The thermodynamic parameters for uranium adsorption on Tp-DAAQ, Tp-AD and Tp-DAQ.

	$\Delta H$ (kJ·mol <sup>-1</sup> )	$\Delta S$ (J·mol <sup>-1</sup> ·K <sup>-1</sup> )	$\Delta G$ (kJ·mol <sup>-1</sup> )		
			303.15 K	313.15 K	323.15 K
Tp-DAAQ	13.36	60.78	-5.07	-5.67	-6.28
Tp-AD	14.29	66.35	-5.82	-6.49	-7.15
Tp-DAQ	11.51	50.02	-3.65	-4.15	-4.65

**Table S9.** The uranium performance comparison of this work and other materials.

Adsorbents	pH	Adsorption capacity (mg·g <sup>-1</sup> )	K <sub>d</sub> (mL·g <sup>-1</sup> )	Ref
TFPT-BTAN-AO	4	427	8.3 × 10 <sup>6</sup>	S1
COF-PDAN-AO	4	410	6.3 × 10 <sup>3</sup>	S2
TzDa-Phos	4	394	5.8 × 10 <sup>3</sup>	S3
ACOF	4.5	169	/	S4
COF-DBS	5	622	1.9 × 10 <sup>4</sup>	S5
COF-TBS	5	243	/	S5
COF-SOH <sub>3</sub>	5	360	/	S6
[NH <sub>4</sub> ] <sup>+</sup> [COF-SO <sub>3</sub> ] <sup>-</sup>	5	851	9.8 × 10 <sup>6</sup>	S6
TzDVa-COOH	5	139.5	/	S7
TpDBD-Phos	5	732.2	2.0 × 10 <sup>4</sup>	S8
JUC-505-COOH	5	464	/	S9
JUC-505-AO	5	395	/	S9
PT-BN-AO	5	548.6	/	S10
BD-TN-AO	5	562	/	S11
TI-COF	5	902	/	S12
COF-OH	5	335.19	/	S13
NDA-TN-AO	5	589.1	/	S14
ECUT-COF-21	5	120	/	S15
DhaTap-COF	5	320	/	S16
DhaTpt-COF	5	1128	/	S16
COF-TpPa-1	6	152	/	S17
COF-TpDb-AO	6	408	3.6 × 10 <sup>8</sup>	S18
M808-4	5.5	418.5	6.5 × 10 <sup>5</sup>	S19
UIO-66-20D	5	350	/	S20
UIO-66-18	8	598.1	/	S21
Tp-DAAQ	6	738.4	7.4 × 10 <sup>3</sup>	<b>This work</b>
Tp-AD	6	834.4	1.0 × 10 <sup>4</sup>	<b>This work</b>
Tp-DAQ	6	382.8	/	<b>This work</b>

## Reference

- S1 W. Cui, C. Zhang, W. Jiang, F. Li, R. Liang, J. Liu and J. Qiu, *Nat. Commun.*, 2020, **11**, 436.
- S2 F. Li, W. Cui, W. Jiang, C. Zhang, R. Liang and J. Qiu, *J. Hazard. Mater.*, 2020, **392**, 122333.
- S3 H. Zhang, S. Wang, J. Yu, Z. Li, J. Lan, L. Zheng, S. Liu, L. Yuan, T. Xiu, J. Wang, X. Wang and W. Shi, *Chem. Eng. J.*, 2023, **463**, 142408.
- S4 X. Li, Y. Qi, G. Yue, Q. Wu, Y. Li, M. Zhang, X. Guo, X. Li, L. Ma and S. Li, *Green Chem.*, 2019, **21**, 649.
- S5 Y. Xu, Z. Yu, Q. Zhang and F. Luo, *Adv. Sci.*, 2023, **10**, 2300408.
- S6 X. Xiong, Z. Yu, L. Gong, Y. Tao, Z. Gao, L. Wang, W. Yin, L. Yang and F. Luo, *Adv. Sci.*, 2019, **6**, 1900547.
- S7 M. Zhou, S. Wang, F. Liu and B. Hu, *Sep. Purif. Technol.*, 2024, **338**, 126501.
- S8 D. Mei and B. Yan, *Adv. Funct. Mater.*, 2024, **34**, 2313314.
- S9 Z. Li, R. Zhu, P. Zhang, M. Yang, R. Zhao, Y. Wang, X. Dai and W. Liu, *Chem. Eng. J.*, 2022, **434**, 134623.
- S10 W. Cui, C. Zhang, R. Xu, X. Chen, R. Yan, W. Jiang, R. Liang and J. Qiu, *ACS EST Water*, 2021, **1**, 440-448.
- S11 C. Zhang, W. Cui, R. Xu, X. Chen, W. Jiang, Y. Wu, R. Yan, R. Liang and J. Qiu, *CCS Chem.*, 2021, **3**, 168-179.
- S12 L. Zhong, X. Feng, Q. Zhang, X. Xie and F. Luo, *Chem. Sci.*, 2024, **15**, 10882.
- S13 X. Liu, X. Wang, W. Jiang, C. Zhang, L. Zhang, R. Liang and J. Qiu, *Chem. Eng. J.*, 2022, **450**, 138062.
- S14 W. Cui, F. Li, R. Xu, C. Zhang, X. Chen, R. Yan, R. Liang and J. Qiu, *Angew. Chem. Int. Ed.*, 2020, **59**, 17684-17690.
- S15 L. Guo, Z. Huang and F. Luo, *Nano Lett.*, 2024, **24**, 14153-14161.
- S16 J. Zhao, L. Zhao, Q. Gao, G. Fu, F. Li, H. Liu and Y. Fa, *Chem. Eng. J.*, 2024, **500**, 157017.
- S17 Z. Li, H. Zhang, X. Xiong and F. Luo, *J. Solid State Chem.*, 2019, **277**, 484-492.
- S18 Q. Sun, B. Aguila, L-D. Earl, C-W. Abney, L. Wojtas, P-K. Thallapally and S. Ma, *Adv. Mater.*, 2018, **30**, 1705479.
- S19 Z. Zhao, R. Lei, Y. Zhang, T. Cai and B. Han, *J. Mol. Liq.*, 2022, **367**, 120514.
- S20 L. Yuan, M. Tian, J. Lan, X. Cao, X. Wang, Z. Chai, J. K. Gibsone and W. Shi, *Chem. Commun.*, 2018, **54**, 370.
- S21 M. Zheng, K. Xuan, S. Yan, Y. Guo, Y. Huang, R. Xu, K. Zhao, Z. Li, X. Li, H. Jiang and Y. Guo, *Sep. Purif. Technol.*, 2024, **339**, 126550.